

REPORT DOCUMENTATION PAGE			Form Approved OMB No. 0704-0188	
Public reporting burden for this collection of information is estimated to average 1 hour per response, including the time for reviewing instructions, searching existing data sources, gathering and maintaining the data needed, and completing and reviewing the collection of information. Send comments regarding this burden estimate or any other aspect of this collection of information, including suggestions for reducing this burden, to Washington Headquarters Services, Directorate for Information Operations and Reports, 1215 Jefferson Davis Highway, Suite 1204, Arlington, VA 22202-4302, and to the Office of Management and Budget, Paperwork Reduction Project (0704-0188), Washington, DC 20503.				
1. AGENCY USE ONLY (Leave blank)	2. REPORT DATE 10 August 1995	3. REPORT TYPE AND DATES COVERED Final Technical Report 1 Feb 93 to 31 Jan 95		
4. TITLE AND SUBTITLE MODELING RESPONSE AND STRENGTH OF MMC UNDER COMPRESSIVE LOADING			5. FUNDING NUMBERS F49620-93-C-0009	
6. AUTHOR(S) Golam M. Newaz Bhaskar S. Majumdar			AFOSR-TR-97	
7. PERFORMING ORGANIZATION NAME(S) AND ADDRESS(ES) Battelle Memorial Institute 505 King Avenue Columbus, Ohio 43201			0311	
9. SPONSORING/MONITORING AGENCY NAME(S) AND ADDRESS(ES) AFOSR/NA 110 Duncan Avenue, Suite B 115 Bolling AFB, DC 20332-8050			10. SPONSORING/MONITORING AGENCY REPORT NUMBER	
11. SUPPLEMENTARY NOTES				
12a. DISTRIBUTION AVAILABILITY STATEMENT Approved for Public Release; Distribution Unlimited.			12b. DISTRIBUTION CODE 19971002 137	
13. ABSTRACT (Maximum 200 words) 2/92-1/93: During this period, extensive research was conducted to study the inelastic deformation of MMCs under monotonic loading for both transverse and longitudinal laminae. Results showed that unidirectional MMC deformation response is strongly controlled by matrix plasticity. this is followed by local instability due to region.fiber buckling and failure of the lamina is due to fiber fracture in this local region. For transverse MMCs, plastic deformation in the matrix is associated with extensive fiber-matrix debonding followed by fiber radial fracture. 2/93-12-94: During this period, research was conducted to develop strength models for MMCs based on failure mechanisms. Both longitudinal and transverse proportional limits (onset of nonlinearity) could be predicted based on properties of the constituents and information about the failure mode that contributes to nonlinear response. Investigation was also carried out to determine the nature of local damage in MMCs with holes under pure compression. These failure modes were studied carefully and it was shown that the Hinckey-Von Mises failure criteria could be effectively used to predict the location of the damage initiation site. Also, during this period, some preliminary experiments were conducted for reversed fatigue loading of longitudinal MMC. this was accomplished with extra effort on the part of the principal investigator within the second year.				
14. SUBJECT TERMS			15. NUMBER OF PAGES	
DTC QUALITY INSPECTED 4			16. PRICE CODE	
17. SECURITY CLASSIFICATION OF REPORT Unclassified	18. SECURITY CLASSIFICATION OF THIS PAGE Unclassified	19. SECURITY CLASSIFICATION OF ABSTRACT Unclassified	20. LIMITATION OF ABSTRACT UL	

**MODELING RESPONSE AND STRENGTH OF MMC UNDER COMPRESSIVE
LOADING
(Statement of Work)**

The primary objectives of this research program were 1) to extensively characterize the inelastic deformation and damage mechanisms in unidirectional MMC in both transverse and longitudinal directions (2/92-1/93), 2) develop micromechanics based strength models for MMC and investigate the inelastic deformation mechanisms around holes in MMC (2/93-1/94), and 3) determine the inelastic deformation mechanisms and associated failure mechanisms under reversed fatigue loading (2/94-1/95).

Program Status

Objectives shown in items 1-2 were successfully completed during the 2/92-12/94 period. The principal investigator left Battelle 12/94. Item 3 was scheduled to be completed in the last year of the three-year program. However, the principal investigator, Dr. Golam Newaz was able to accomplish some preliminary experiments for item 3, prior to his departure from Battelle. As the program was canceled, research for item 3 was not carried out to completion. Overall, the program objectives for the first two years were exceeded and excellent research results were published in the literature (copies of representative papers are enclosed). Preliminary results from item 3 were also published.

Summary of Accomplishments

2/92-1/93: During this period, extensive research was conducted to study the inelastic deformation of MMCs under monotonic loading for both transverse and longitudinal laminae.

Results showed that unidirectional MMC deformation response is strongly controlled by matrix plasticity. This is followed by local instability due to fiber buckling and failure of the lamina is due to fiber fracture in this local region. For transverse MMCs, plastic deformation in the matrix is associated with extensive fiber-matrix debonding followed by fiber radial fracture.

2/93-12/94: During this period, research was conducted to develop strength models for MMCs based on failure mechanisms. Both longitudinal and transverse proportional limits (onset of nonlinearity) could be predicted based on properties of the constituents and information about the failure mode that contributes to nonlinear response.

Investigation was also carried out to determine the nature of local damage in MMCs with holes under pure compression. These failure modes were studied carefully and it was shown that the Hinckey-Von Mises failure criteria could be effectively used to predict the location of the damage initiation site.

Also, during this period, some preliminary experiments were conducted for reversed fatigue loading of longitudinal MMC. This was accomplished with extra effort on the part of the principal investigator within the second year and without any extra costs for that year.

SELECTED RESEARCH PUBLICATIONS

Presented at ASTM Symposium on "The Prediction of MMC", 1994
To appear in an ASTM STP.

INELASTIC DEFORMATION MECHANISMS IN SCS-6/Ti 15-3 MMC LAMINA UNDER COMPRESSION

Golam M. Newaz and Bhaskar S. Majumdar**

Battelle Memorial Institute

Columbus, Ohio 43201

ABSTRACT

An investigation was undertaken to study the inelastic deformation mechanisms in $[0]_8$ and $[90]_8$ Ti 15-3/SCS-6 lamina subjected to pure compression. Monotonic tests were conducted at room temperature (RT), 538°C and 650°C. Results indicate that mechanical response and deformation characteristics were different in monotonic tension and compression loading whereas some of those differences could be attributed to residual stress effects. There were other differences because of changes in damage and failure modes. The inelastic deformation in the $[0]_8$ lamina under compression was controlled primarily by matrix plasticity, although some evidence of fiber-matrix debonding was observed. Failure of the specimen in compression was due to fiber buckling in a macroscopic shear zone (the failure plane). The inelastic deformation mechanisms under compression in $[90]_8$ lamina were controlled by radial fiber fracture, matrix plasticity and fiber-matrix debonding. The radial fiber fracture was a new damage mode observed for MMCs. Constitutive response was predicted for both the $[0]_8$ and $[90]_8$ laminae, using AGLPLY, METCAN and Battelle's Unit Cell FEA model. Results from the analyses were encouraging.

INTRODUCTION

Titanium based metal matrix composites (MMCs) offer excellent potential for high temperature applications which require a combination of high temperature strength, stiffness and toughness. Current advances in processing of this class of materials have made them

** Currently with Universal Energy Systems, Inc., Dayton, Ohio

technologically viable for their use in various engine and aerothermal applications. Considerable research to date has been conducted in characterizing SiC fiber-reinforced titanium composites [1-9]. The references reflect only a small number of representative publications from a much larger pool.

An important feature of MMCs is that there is significant difference in the coefficient of thermal expansion between the fiber and matrix; the matrix has a larger coefficient of thermal expansion. Consequently, large compressive radial stresses build up at the interface between the matrix and the fiber as the composite is cooled from the processing temperature. Of course, fiber volume fraction affects the magnitude of the residual stresses. On the other hand, the axial and circumferential stresses in the matrix are both tensile in nature. This combination of stresses sets up yielding or near yielding conditions in the matrix immediately adjacent to the fiber. A consequence of such high stresses is that micro-yielding may occur well before macroscopic yield is observed when the MMC is loaded mechanically. In addition, the strength of the bond between the fiber and the matrix has been shown by many researchers [5,7,9] to be weak in the composite. Also, the presence of the reaction zone adds another dimension to the complex deformation characteristics in these composites under applied loading.

The loading mode which has received most attention by researchers in the field is tensile loading. Although, this is certainly the dominant loading mode for the application of the fiber reinforced MMCs, compressive loading in the application of these structural materials is a definite possibility for various components. Compression on one surface is a reality in bending. Furthermore, in the case of reversed fatigue loading, the composite will experience compressive loading in part of the cycle.

It is also anticipated that structural design engineers will require design allowables for tensile, compressive and shear properties. Compressive loading has not received much attention to date for high temperature composites. Past studies on Boron/Aluminum composites concentrated on their longitudinal compression behavior [10]; however, their transverse compression behavior was not studied. Understanding of the evolution of damage and failure modes under compressive loading of the MMC at high temperature is seriously lacking. Considerable research is needed to clarify and resolve the micromechanics issues

for compressive response. It is also necessary to complement experimental efforts with analytical ones to predict the constitutive response of the MMC under compressive loading since such efforts are not under consideration in any of the major high temperature programs.

Often damage accumulates in local regions in a structure due to high stresses and strains. If the damage reaches a critical level, it can lead to failure of the structure. Constitutive models are essential to evaluate local stress and strain fields developed due to global structural loading. However, rational constitutive models can be only developed if the mechanisms for material deformation and damage development can be clarified and used to develop the models. Analytical constitutive models often require an assumption of ideal microstructures and may simplify the problem to a level where realism is compromised, particularly for heterogeneous materials like composites. A computational framework on the other hand provides much versatility and can be effectively utilized provided deformation mechanisms are properly accounted for. For MMC structures subjected to compressive loading (a situation which exists even in the case of simple bending), constitutive modeling under compressive loading is a clearly defined need. Clarification of damage modes and deformation mechanisms are equally important compared with constitutive modeling and are integrally related. The material deformation characteristics and modeling for monotonic loading constitutes the basic requirements for structural analysis.

Inelastic deformation is critical in that its initiation and evolution contributes to the failure of a structural part. Proper constitutive models can only be developed when actual inelastic deformation mechanisms can be ascertained and incorporated into modeling.

In recognition of the need to clarify the inelastic deformation mechanisms under compressive loading, a brief investigation was undertaken to monitor the initiation and progression of damage in the SCS-6/Ti 15-3 MMC for both $[0]_8$ and $[90]_8$ laminae subjected to monotonic compressive loads, particularly at elevated temperature. This small effort was only part of a much larger effort for damage evaluation under cyclic loading in titanium-based MMCs which is covered in a separate report. This information will be extremely valuable for constitutive and damage modeling for this class of materials. Results were also compared with tension response and corresponding deformation mechanisms.

EXPERIMENTAL ASPECTS

The material tested was an 8-ply unidirectional SCS-6/Ti 15-3 composite, approximately 1.99-mm thick, with a fiber volume fraction of approximately 0.35. The SCS-6 (SiC) fiber diameter is approximately 140 μm , and it contains alternating outer layers of C and Si, which protect the fiber from damage during handling. The Ti 15-3 alloy is a metastable body centered cubic (bcc) beta Ti-alloy, the bcc phase being stabilized by V. The material is metastable because hexagonal close packed (hcp) alpha phase, which is the stable room temperature phase of pure Ti, precipitates when the material is held at temperatures as low as 400°C for long periods of time.

[0]₈ and [90]₈ rectangular test specimens were machined from the unidirectional panel using an electric-discharge machining (EDM) technique, with specimen dimensions of 2.0 mm x 10.2 mm x 104.1 mm. The gage length was 25.4 mm. The specimens were mechanically polished after EDM machining to minimize any damage associated with the machining. All specimens were tested in the as-fabricated condition, i.e., no heat-treatment was performed prior to the testing. Tests were conducted at room temperature, 538°C (1000°F) and 650°C (1200°F).

Specimens were gripped using friction grips, and loaded on a servohydraulic testing machine at a strain rate of approximately 0.004/sec. Compression testing was done using a Battelle developed compression fixture as shown in Figure 1 which uses buckling guides. The longitudinal strains were measured using extensometer.

A few tests were conducted without buckling guides, particularly for [0]₈ specimens. Longitudinal macro-buckling of the specimen is shown in Figure 2. A failure mode typically not observed in MMCs, i.e. delamination, was also observed. Premature buckling may not allow evaluation of proper mechanical response and properties at higher stress or strains. Therefore, lateral restraint for unidirectional higher strength MMCs are essential to develop a good understanding of key deformation mechanisms under pure compressive loading.

Following mechanical testing, most of the compression specimens were not loaded to failure. A number of specimens were polished at the edges. A fairly complex polishing procedure has been developed at Battelle for evaluating MMCs to preserve the characteristics

of deformation. Repeated polishing was performed on a few tested and untested samples to confirm that any cracking, debonding, or slip bands was due to deformation alone, and not associated with the polishing procedure or manufacturing. Specimens were etched using Kroll's reagent, which was found to be effective in revealing slip bands both at surface and subsurface locations. Metallographic specimens were examined optically and key deformation characteristics were photographed.

The overall test matrix is given in Table 1. The study did not allow for any statistical property evaluation.

RESULTS AND DISCUSSION

Mechanical Behavior Evaluation

Longitudinal Lamina

The typical stress-strain response including unloading for a $[0]_8$ specimen is shown in Figure 3. The compression test result without buckling guides is also shown in the same figure. The elastic modulus in tension and compression were similar, ranging between 175-179 GPa. Also, the corresponding tension data is presented in the same plot. It may be noted that the compression capability of the $[0]_8$ lamina is significantly higher than the tension case both in terms of (1) the onset of nonlinearity and (2) the higher ultimate strength (when premature buckling is avoided). The compression specimen was not loaded to failure. However, experimental efforts suggest that the compression strength will be quite high. In the absence of restraint for buckling, it is clear that premature buckling takes place resulting in no useful information in the nonlinear deformation regime. The failure mode for compression without buckling guides will be discussed in the Microstructural Evaluation section. The unloading line is parallel to the elastic loading line for the $[0]_8$ composite and indicate that the deformation response is controlled primarily by plastic deformation. The mechanical responses at 538 C and 650 C are included in Figure 4 along with room temperature response. Table 2 provides data on the effect of temperature on the proportional

limit and modulus. The decrease in modulus and proportional limit are due to the decrease in flow properties of the matrix at elevated temperature.

The onset of non-linear deformation at RT in compression (approx. 2200 MPa) was significantly higher than in tension (approx. 980 MPa). This difference is due to a residual tensile stress in the matrix; calculations show [11] that for this system the axial residual stresses at room temperature (RT) are approximately 412 MPa in the matrix at the fiber-matrix interface, and -1000 MPa in the fiber. Assuming an elastic one-dimensional response, the residual axial stress can be calculated using the formula $S_r = [(|S_c| - |S_t|)/2] * E_m/E_c$, where S_c and S_t are the measured proportional limits in compression and tension, and E_m and E_c are matrix and composite moduli. Using this formula, the tensile axial residual stress in the matrix is calculated to be 335 MPa.

Transverse Lamina

Figure 5 shows the typical stress-strain response of the $[90]_8$ lamina for the three different temperatures, namely, room temperature, 538°C (1000°F) and 650°C (1200°F). In each case, the specimens were unloaded in the nonlinear regime. There is a progressive loss in elastic modulus and proportional limit as a function of temperature as given in Table 3. The distinct knee observed in tension for the onset of nonlinearity in the $[90]_8$ lamina (Figure 5) is clearly absent in the case of compression. The onset of nonlinearity in the tension stress-strain curve was attributed to fiber-matrix debonding - a dominant damage mechanism for the $[90]_8$ MMC lamina. Note the large work hardening period for the MMC, extending from approximately 0.5 percent strain to approximately 1 percent strain. This period was much longer than for the matrix material.

The room temperature and 538°C compression stress-strain results are compared in Figure 6 with those of the tension case to accentuate the difference in the response of the same SCS-6/Ti 15-3 composites under different loading conditions. This plot also contains the pure matrix stress-strain response in tension at room temperature and at 538°C. There are two important observations that can be made from this comparison; 1) the initial elastic or tangent moduli under tension and compression are similar, and 2) the proportional limits

in compression are higher than for their corresponding tension counterparts. The higher proportional limit can be explained by the presence of a beneficial tensile residual stress which must be overcome in compression before a compressive proportional limit is reached. A matrix average radial residual compressive stress of ~ 190 MPa at room temperature, estimated from the proportional limits in tension and compression, compares well with a prediction of ~ 200 MPa using Finite Element Analysis (FEA).

The unloading characteristics for the $[90]_8$ specimens under compression are quite different than those observed in tension. The initial unloading line is parallel to the initial loading line in compression signifying plastic deformation at work. The offset strains in each case for all temperatures is significantly large (Figure 5). Further unloading results in a somewhat more compliant behavior as zero load is approached.

Microstructural Evaluation

Longitudinal Lamina

Optical photomicrographs of replicas taken from polished specimens show the presence of extensive matrix plasticity in the lamina (Figure 7). Fiber-matrix debonding is also evident at higher strain levels within the ply. These observations were only made at room temperature. The failure due to fiber buckling in an unrestrained test is shown in Figure 8. The fibers break in a shear plane within the gage section. This failure is indicative of a buckling instability due to compressive load.

Transverse Lamina

Optical photomicrographs of specimens polished after testing revealed the nature of deformation characteristics under compressive loading quite clearly. The initial deformation mechanism under monotonic compressive loading is found to be matrix plasticity along the loading axis between fibers as shown in Figure 9 for a specimen tested at room temperature. This appears to be a dominant mechanism controlled by high strains between the fibers

within a ply along the loading line during compression and less plasticity between the adjacent plies. This partitioning of plasticity likely was responsible for the high work hardening that were observed for the compression specimen (Figure 6). It may be recalled that in the case of tension, there was only a knee associated with debonding and the smooth behavior under compression as shown in Figure 6 was absent. The slip lines are considerably more prominent compared to the similar slip lines observed in the tension case at similar locations [7,9]. In the case of tension, the initial micro-plasticity is followed by fiber-matrix debonding at the fiber poles at the onset of departure from the linear elastic response (knee). In the case of compression, the nonlinearity is a smooth one (Figure 6) without any abrupt change from linearity. Debonding, as observed in the tension case at the two poles of a fiber, is absent in the compression case, as the matrix is in compression at the poles of the fiber (top and bottom points on the fibers in Figure 9).

Careful observation also reveals a very interesting damage condition in the composite under compression. There are radial cracks within the fibers oriented primarily along the compression loading axis which form after the initial slip lines have developed in the matrix as mentioned earlier. Reaction zone cracks (RZC) are also observed. These damage modes are depicted in Figure 10. This damage mode was reported earlier by Newaz and Majumdar [12-14]. Radial fiber cracking is indicative of the low radial fiber strength which may be related to the soft carbon core in the SCS-6 fiber and the columnar grain structure of the CVD deposited SiC with grain boundary facets oriented radially. These cracks are not observed in as-received materials and were not observed in the tension loading mode.

In the nonlinear regime, further compressive deformation of the composite results in the development of bulk plasticity in the matrix with extensive networks of shear slip bands. This is illustrated in the Figures 11a and 11b for specimens tested at 538°C and 650°C. These micrographs were taken under polarized light to capture the active slip bands. Also, it may be noted that there is significant debonding of fiber and matrix at 90-degree locations from the loading axis. This is in contrast to the debonding at the poles for the tension case. This is clearly shown in Figures 12a and 12b. Qualitatively, the debonding in compression can be attributed to high local tensile transverse strains at the fiber-matrix interface which develop during compressive deformation of the specimen. Shear strains at the fiber-matrix

interface are also expected. However, precise computational analysis will be required to determine the contribution of normal and shear strains to the debonding phenomena observed.

The transverse compression response is compared with the transverse tension response in Table 4 in terms of the leading inelastic deformation mechanisms. Although, the radial cracking of fiber in compression is a concern, it may be noted that the most debilitating damage, i.e. one that occurs at a fairly low strain level, is fiber-matrix debonding under tension. Radial fiber cracking is observed in compression at a strain level of 0.007 whereas debonding under tension initiates around a strain level of 0.003.

The sequence and location of damage development under tension and compression can explain the different stress-strain responses of the composite. Furthermore, this specific behavior with regard to the "knee" can be rationalized based on the effect of debonding orientation on the mechanical response of the composites in tension and compression as illustrated in Figure 18. Reaction zone cracks and debonding which are perpendicular to load axis as in the case in tension are anticipated to have a larger effect on compliance.

ANALYTICAL CONSIDERATIONS

Within the scope of the compression investigation, an effort was made to determine the suitability of a few constitutive models to predict the stress-strain response under monotonic compression. Our effort was only confined to the transverse constitutive response.

A unique set of micromechanics equations have been developed by NASA researchers for high temperature metal matrix composites [15]. These equations coupled with a set of thermoviscoplastic nonlinear multifactor relations developed by these researchers [16] are consolidated into a computational code titled METCAN. It treats the material nonlinearity at the constituent level, where the material's non-linear time-temperature-stress dependence is modeled using power-law type multifactor interaction relationships. Although the model can account for interface damage in a limited way, by changing the mechanical properties of the interphase region (the region consisting of the reaction-zone and the interfaces), it cannot predict a priori what the interphase property should be. METCAN was used to predict the

stress-strain behavior for both $[0]_8$ and $[90]_8$ SCS-6/Ti 15-3 laminae under both room and elevated temperature. These results are presented in Figures 13a and 13b. The correlations are quite good and are encouraging. METCAN is not suitable for unloading and therefore, no attempt was made to predict the unloading response.

Also, the AGLPLY code was used (continuum plasticity based model by Dvorak and Baheiel-Din [17]) which is based on a vanishing fiber diameter model, and can be used effectively to predict lamina and laminate responses from the elastic-plastic responses of the matrix and fiber materials. The primary drawback of the model is that it cannot account for damage. Comparison of the AGLPLY predictions with experimental data for the $[0]_8$ MMC at room temperature is given in Figure 14. In the predictions, the $[90]_8$ MMC are compared with experimental data in Figure 15. The figure also includes experimental data obtained by Lerch [18] at NASA Lewis using a 32-ply MMC without any buckling guides. While the experimental data from the two investigations are in agreement, the AGLPLY predictions are not good in the inelastic regime of deformation. Rather, AGLPLY appeared to mimic the matrix behavior. The inadequacy of AGLPLY prediction may be related to the assumption of vanishing fiber diameter which averages out the microstructure and cannot account for the way plasticity is partitioned between different regions of the MMC.

Battelle's finite element computational unit cell model developed by Brust, et al. [11] was also used to predict the stress-strain response of $[0]_8$ and $[90]_8$ laminae for the room temperature case. The following analytical aspects were involved in the model: (1) 2-D generalized plane-strain conditions, (2) periodic boundary conditions, (3) classical thermal plasticity for the matrix, whose property was assumed to be independent of position, (4) thermo-elastic properties of the fiber, and (5) the fiber-matrix interface was modeled as a discrete interface. For the case of simulating constraints due to the buckling guides, transverse stiffening was modeled using springs with appropriate constants. The results are shown in Figures 16 and 17. The correlation of experimental and predicted results are quite good. Notably, the unloading response was captured for the more complex $[90]_8$ stress-strain response. The compliance change late in unloading at low loads requires further clarification. This work is currently underway at Battelle.

CONCLUSIONS

Based on the current investigation, the following conclusions can be reached.

1. Inelastic deformation in the $[0]_8$ lamina under compression is controlled primarily by matrix plasticity. Some fiber-matrix debonding is also observed.
2. Premature buckling can result if restraints (buckling guides) are not used for $[0]_8$ lamina in compression.
3. Macroscopic instability resulting in fiber failure by buckling within a shear zone in the gage section of the specimen was observed in longitudinal compression for the $[0]_8$ lamina.
4. The mechanical response and deformation characteristics in SCS-6/Ti 15-3 $[90]_8$ lamina are different in monotonic tension and compression. The characteristic early knee associated with fiber-matrix debonding in the stress-strain response of the $[90]_8$ lamina under tension is absent in the case of the monotonic compressive response.
5. There is a marked decrease in proportional limit and increased ductility as the temperature is increased for both the $[0]_8$ and the $[90]_8$ SCS-6/Ti 15-3 laminae in compression. These can be rationalized in terms of matrix flow properties.
6. Radial fiber fracture at the carbon core in SCS-6 fibers is a distinct damage mechanism observed under compressive loading in the $[90]_8$ lamina. The transverse compression capability of the SCS-6 fibers are anticipated to be low due to the columnar structure of the SCS-6 fiber. Extensive matrix plasticity and debonding are also dominant mechanisms under compression. These mechanisms are observed at elevated temperature as well.

7. AGLPLY analysis predicts the $[0]_8$ stress-strain response quite well, but does not predict the $[90]_8$ response as well. Also, computational results using NASA's METCAN and Battelle's Unit Cell Model adequately predict the stress-strain response of both the $[0]_8$ and $[90]_8$ laminae under compression.

ACKNOWLEDGEMENT

Funding for this work was provided by AFOSR. Dr. Walter Jones was the program monitor. The authors wish to thank Mr. Norm Frey, Mr. Glen Foster and Mr. Sam Naboulsi of Battelle Memorial Institute for their assistance in testing, microscopy and stress analysis.

REFERENCES

1. Sun, C. T., "Modeling Continuous Fiber Metal Matrix Composite as an Orthotropic Elastic-Plastic Material", ASTM STP 1032, 1989, pp. 148-160.
2. Lerch, B. A. and Saltsman, J. F., "Tensile Deformation Damage in SiC Reinforced Ti-15V-3Cr-3Al-3Sn", NASA Technical Memorandum 103620, April, 1991.
3. Majumdar, B. S. and Newaz, G. M., "Thermomechanical Fatigue of a Quasi-Isotropic Metal Matrix Composite", ASTM STP 1110, 1991, pp. 732-752.
4. Newaz, G. M., Majumdar, B. S. and Brust, F. W., "Thermal Cycling Response of Quasi-Isotropic Metal-Matrix Composites", ASME J. of Engg. Materials and Technology, April, 1992, pp. 156-161.
5. Johnson, W. S., Lubowinski, S. J. and Highsmith, A. L., "Mechanical Characterization of Unnotched SCS-6/Ti-15-3 Metal Matrix Composites at Room Temperature", ASTM STP 1080, pp. 193-218, 1990.
6. Nimmer, R. P., Bankert, R. J., Russell, E. S., Smith, G. A. and Wright, K. P., "Micromechanical Modeling of Fiber/ Matrix Interface Effects in Transversely Loaded SiC/Ti-6-4 Metal Matrix Composites Technology and Research, Vol. 13, #1, 1991, pp. 3-13.
7. Majumdar, B. S. and Newaz, G. M., "Inelastic Deformation in Metal Matrix Composites: Plasticity and Damage Mechanisms", Philosophical Magazine, London, 1992, Vol. 66, #2, pp 187-212.
8. Gunawardena, S. R., Jansson, S. and Leckie, F. A., "Transverse Ductilities of Metal Matrix Composites", AD-22, ASME Winter Annual Meeting, Atlanta, December, 1991, pp. 23-30.
9. Newaz, G. M. and Majumdar, B. S., "Deformation and Failure Mechanisms in MMC", AD-22, ASME Winter Annual Meeting, Atlanta, 1991, pp. 55-66.
10. Lamothe, R. M. and Nunes, J., "Evaluation of Fixturing for Compression Testing of Metal Matrix and Polymer Matrix Composites", ASTM STP 808, R. Chait and R. Paprino, Eds., 1983, pp. 241-253.
11. Brust, F. W., Majumdar, B. S., and Newaz, G. M., "Constitutive and Damage Response of Ti 15-3/SCS-6 MMC," presented at the ASTM Conference on Fatigue and Fracture, Pittsburgh, PA, (May 4-5, 1992).

12. Newaz, G. M. and Majumdar, B. S., "Failure Modes in Transverse MMC Lamina Under Compression" accepted for publication in the J. of Materials Science & Letters, UK, December, 1992.
13. Newaz, G. M. and Majumdar, B. S., "Inelastic Deformation Mechanisms in a Transverse MMC Lamina Under Compression," AD-Vol. 27, Fracture and Damage, ASME Winter Annual Meeting, Anaheim, 1992, pp. 77-84.
14. Majumdar, B. S. and Newaz, G. M., "Inelastic Deformation Mechanisms in MMC: Compression and Fatigue," HITEMP Review, NASA Conference Publication 10104, 1992, p. 49-1.
15. Hopkins, D. A. and Chamis, C. C., "A Unique Set of Micromechanics Equations for High-Temperature Metal Matrix Composites," ASTM STP 964, 1988, pp. 159-176.
16. Chamis, C. L. and Hopkins, D. A., "Thermoviscoplastic Nonlinear Constitutive Relationships for Structural Analysis of High-Temperature Metal Matrix Composites," ASTM STP 964, 1988, pp. 177-196.
17. Dvorak, G. J. and Bahei-El-Din, Y. A., J. Applied Mechanics, Vol. 49, 1982, pp. 327-335.
18. Lerch, B. A. Private communication, NASA-LeRC, Cleveland, December, 1992.

TABLE 1. COMPRESSION TEST MATRIX
(SCS-6/Ti 15-3)

Layup	Number of Specimens	Temperature	Comments
[0] ₈	1	RT	Stress-strain, edge replication
	2	RT	Intermediate unloading
	1	RT	Without guides
	1	538 C	Stress-strain, unloading
	1	650 C	Stress-strain, unloading
[90] ₈	1	RT	Stress-strain
	2	RT	Intermediate unloading
	1	RT	Edge replication
	1	538 C	Stress-strain, unloading
	1	650 C	Stress-strain, unloading

TABLE 2. $[0]_8$ SCS-6/Ti 15-3 PROPERTIES IN COMPRESSION

Temperature	Young's Modulus (GPa)	Proportional Limit	
		Stress (MPa)	Strain
RT	179	2200	0.012
538 C	170	1200	0.007
650 C	150	600	0.004

TABLE 3. $[90]_8$ SCS-6/Ti 15-3 PROPERTIES IN COMPRESSION

Temperature	Young's Modulus (GPa)	Proportional Limit	
		Stress (MPa)	Strain
RT	125	697	0.006
538 C	108	428	0.004
650 C	92	276	0.003

TABLE 4. DEFORMATION MECHANISMS IN TENSION AND COMPRESSION

[90] _g SCS-6/Ti 15-3					
Inelastic Deformation Mechanisms	Tension		Compression		
	Strain	Stress, MPa	Strain	Stress, MPa	Stress, MPa
Plastic Slip Band	0.002	225	0.002*		225*
Debonding	0.003-0.005	280-340	0.006-0.008		700-900
Reaction Zone Cracks	0.005	350	0.006		700
Radial Fiber Cracking	--	--	0.006-0.008		700-900
Extensive Matrix Plasticity	> 0.006	400	> 0.01		900

* data not retrievable at earlier strain/stress levels because of loss of replica

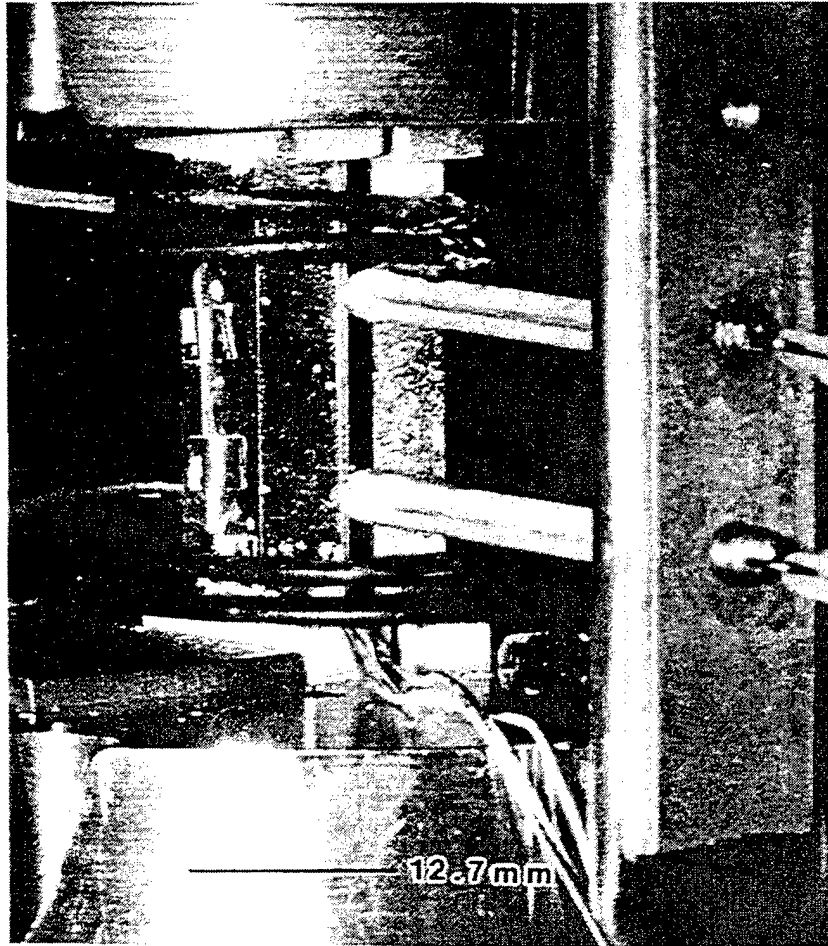


FIGURE 1. COMPRESSION TEST SETUP

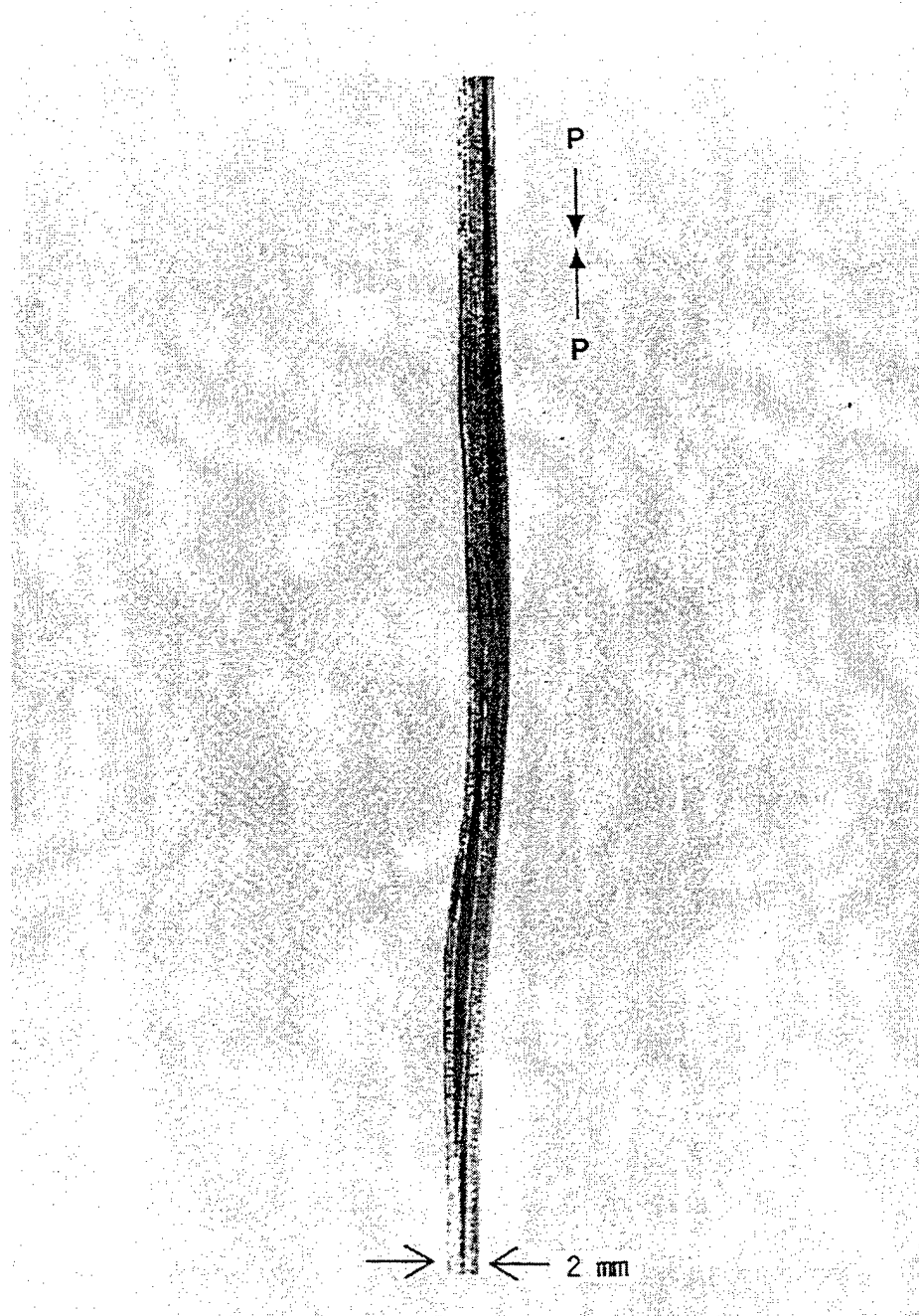


FIGURE 2. MACROBUCKLING OF UNIDIRECTIONAL SPECIMEN WITHOUT RESTRAINTS, SUBJECTED TO COMPRESSION.

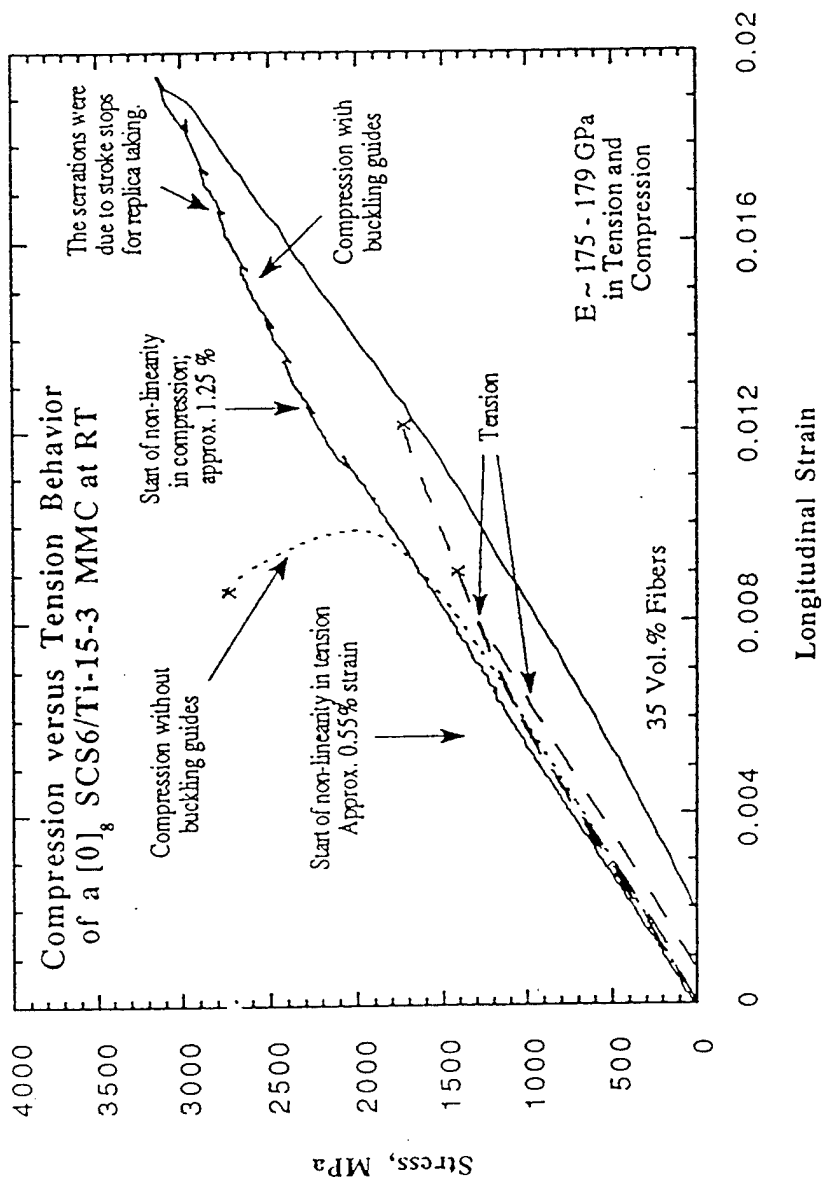


FIGURE 3. TYPICAL STRESS-STRAIN RESPONSE OF $[0]_8$ LAMINA IN COMPRESSION. ALSO INCLUDES TENSION RESULTS FOR THE SAME LAMINA.

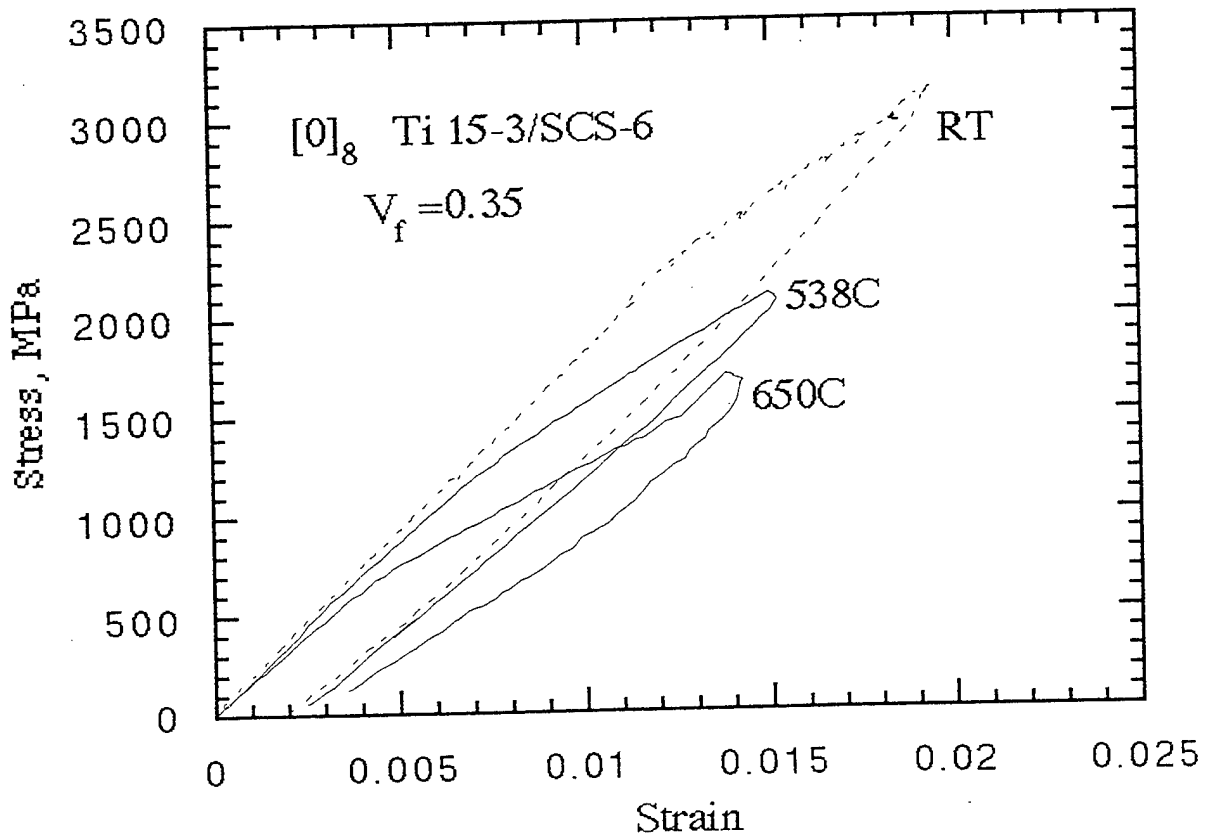


FIGURE 4. MECHANICAL RESPONSE AT ELEVATED TEMPERATURE FOR $[0]_8$ LAMINA IN COMPRESSION

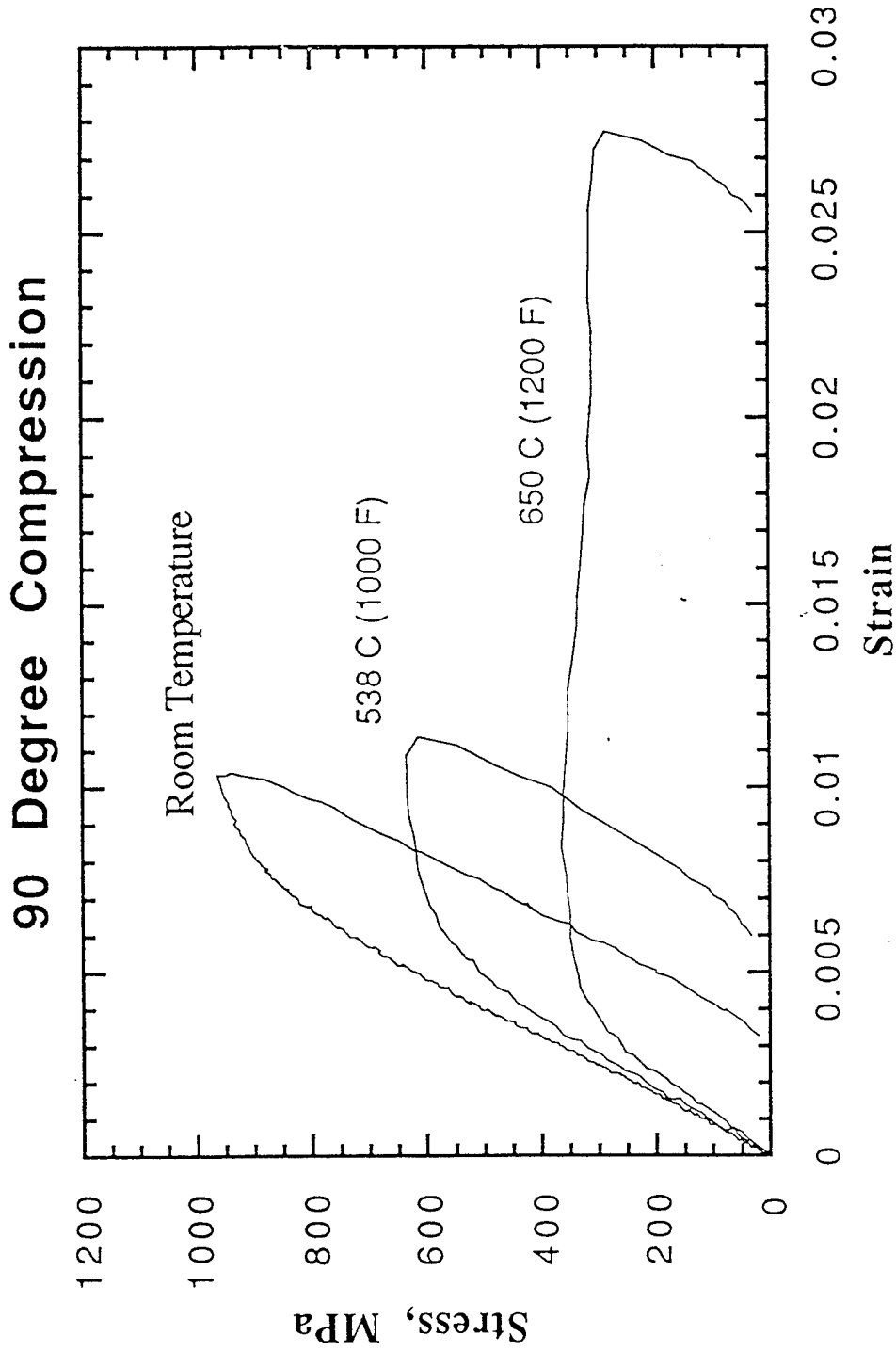
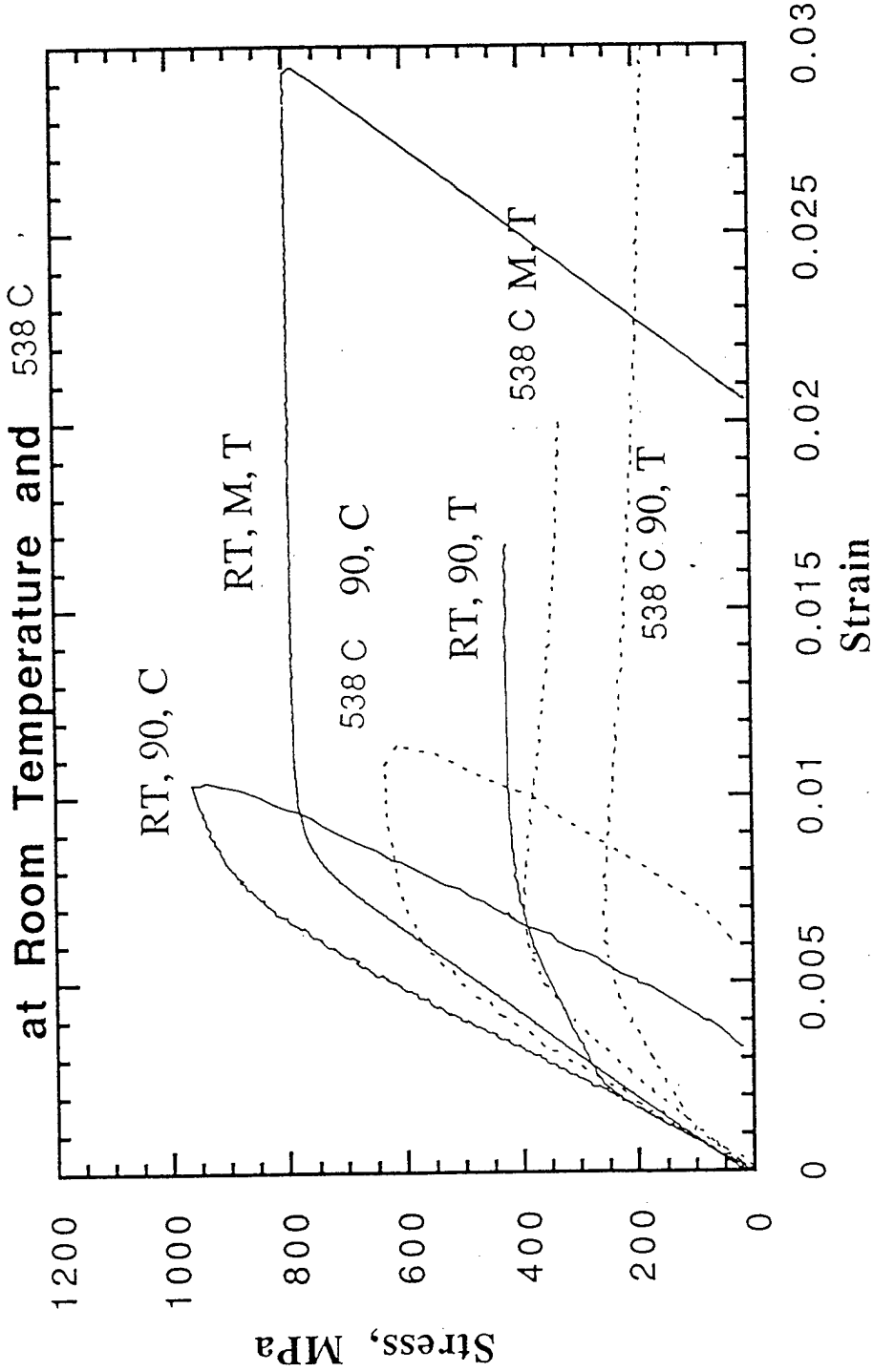


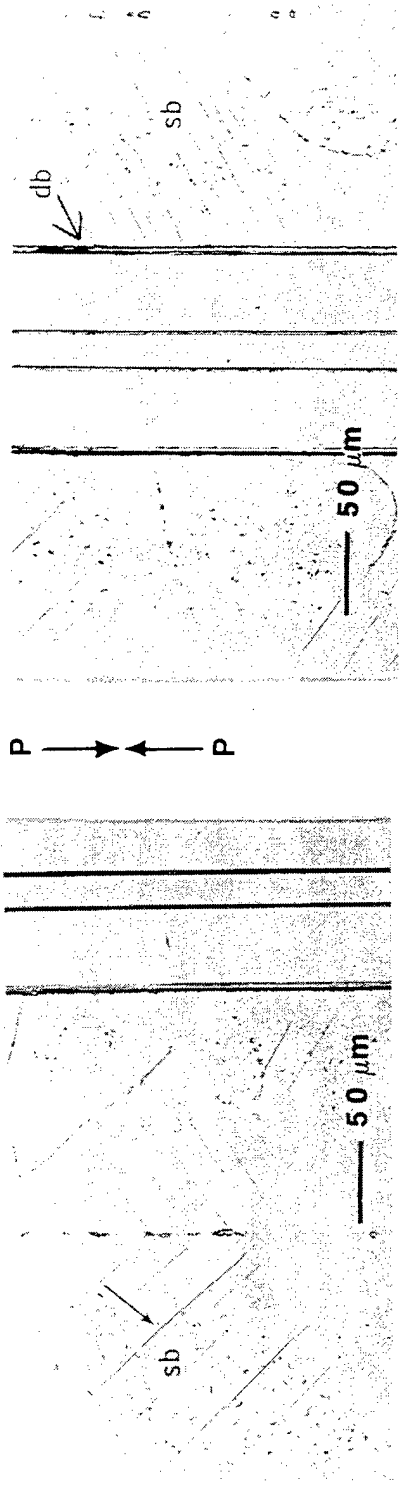
FIGURE 5. MECHANICAL RESPONSE OF $[90]_8$ LAMINA IN COMPRESSION

90-Compression, 90-Tension, & Matrix
at Room Temperature and 538 C

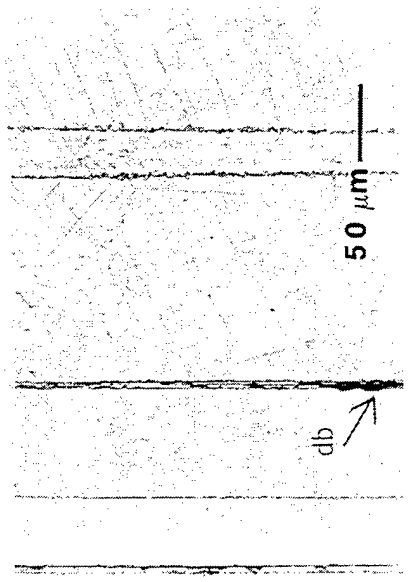


T = Tension, C=Compression, M = Matrix

FIGURE 6. COMPARISON OF COMPRESSION AND TENSION RESPONSE OF [90]₈ LAMINA. MATRIX BEHAVIOR IN TENSION IS SHOWN TOO.



Strain 0.01 Strain 0.013



Strain 0.018

FIGURE 7. PLASTIC SLIP BANDS (sb) AND DEBONDING (db) IN $[0]_8$ LAMINA AT RT IN COMPRESSION.

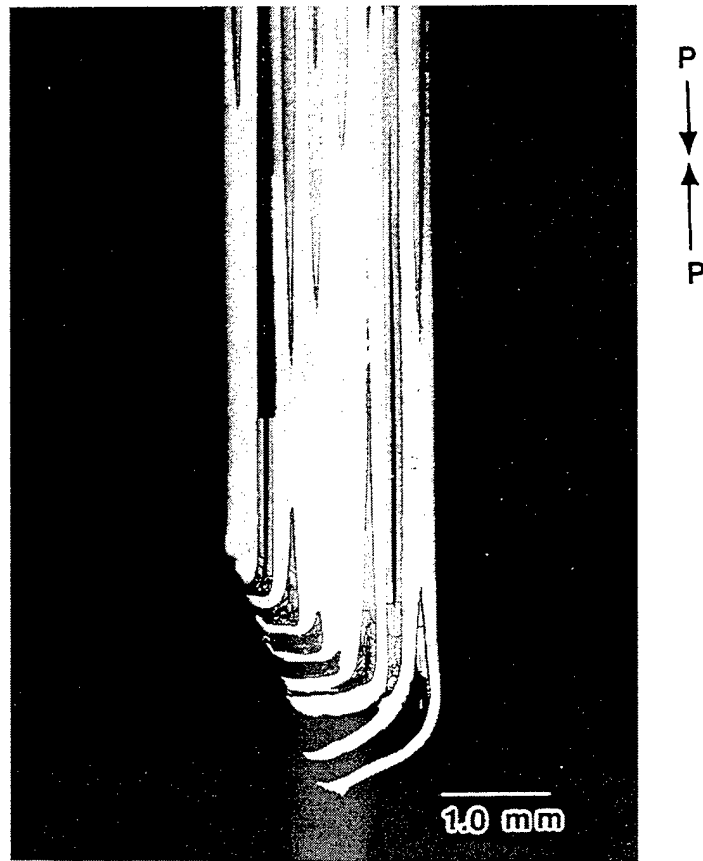
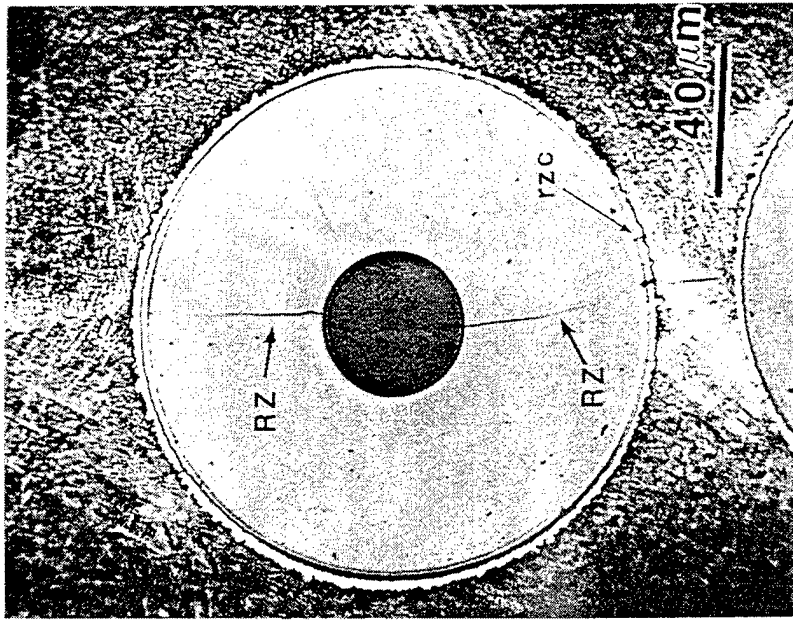
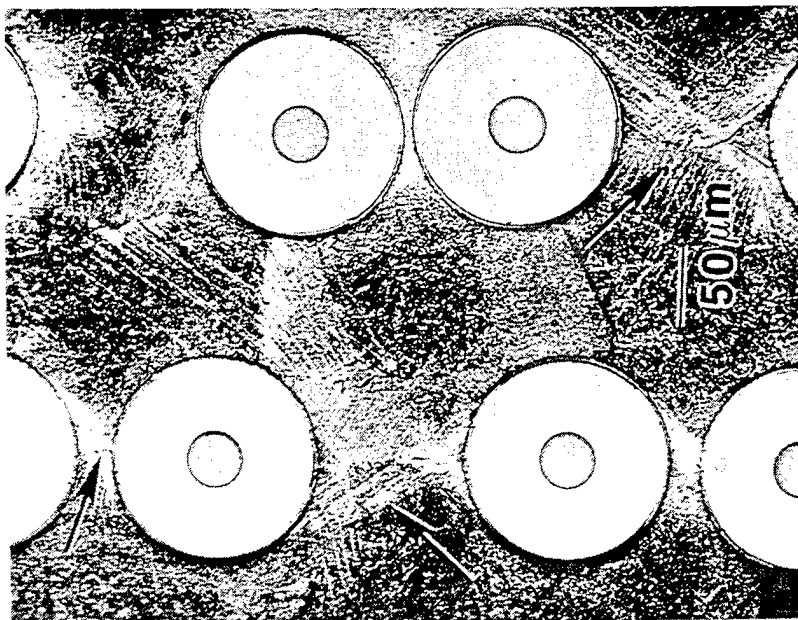


FIGURE 8. FIBER BUCKLING IN $[0]_8$ LAMINA IN COMPRESSION AT RT.



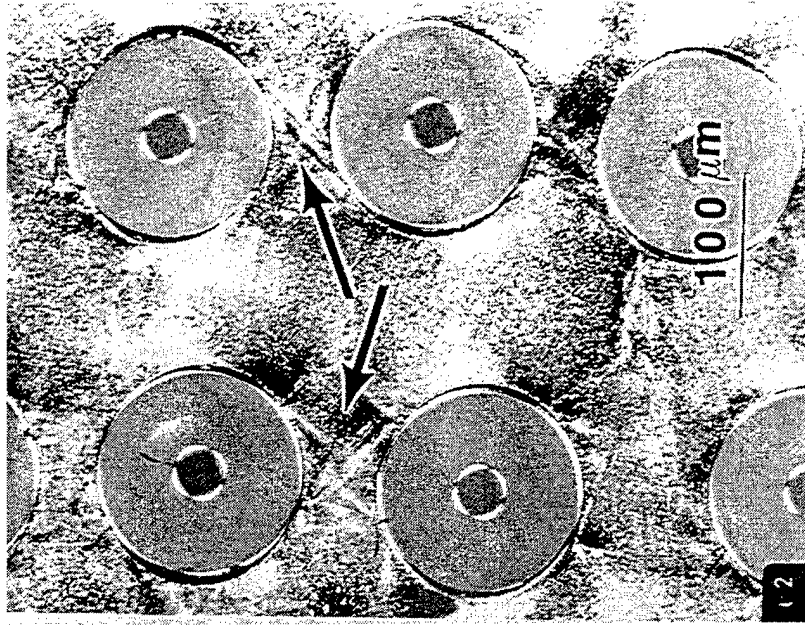
RADIAL CRACKS IN SCS-6 FIBER IN A [90]₂ Ti 15-3/SCS-6, LAMINA UNDER COMPRESSION AT ROOM TEMPERATURE. LOADING IS UP AND DOWN.

FIGURE 10.



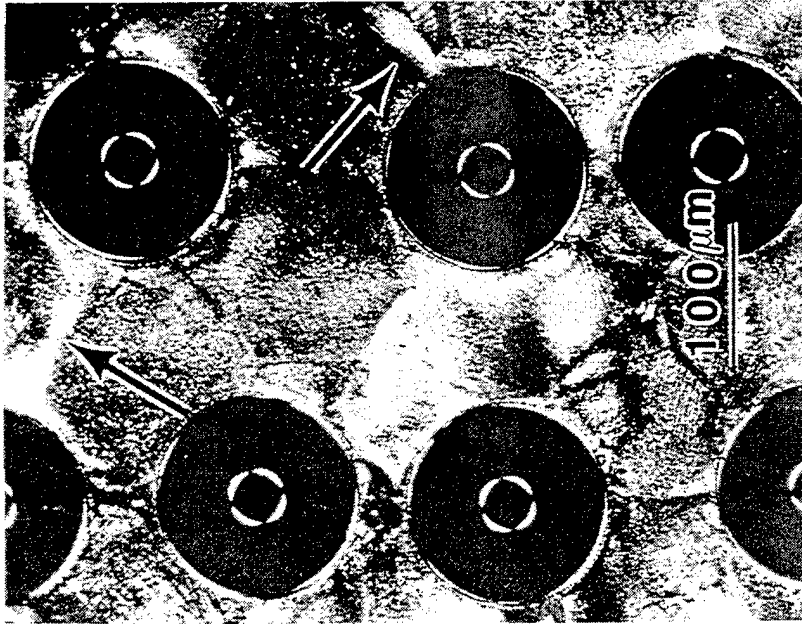
MATRIX PLASTICITY BETWEEN FIBERS IN Ti 15-3/SCS-6 [90]₂ LAMINA UNDER COMPRESSION AT ROOM TEMPERATURE. LOADING IS UP AND DOWN.

FIGURE 9.



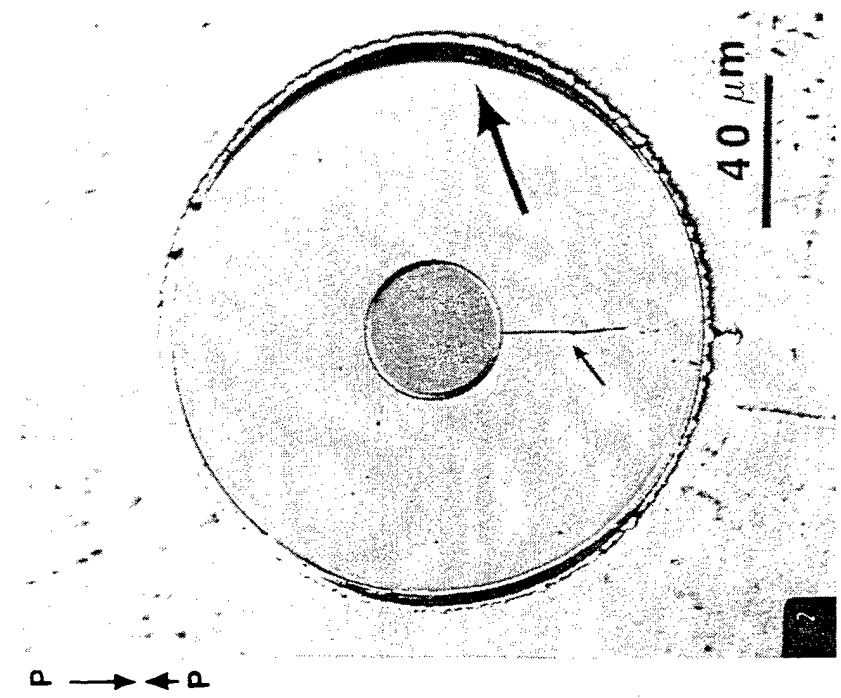
b) 650°C

P → ← P

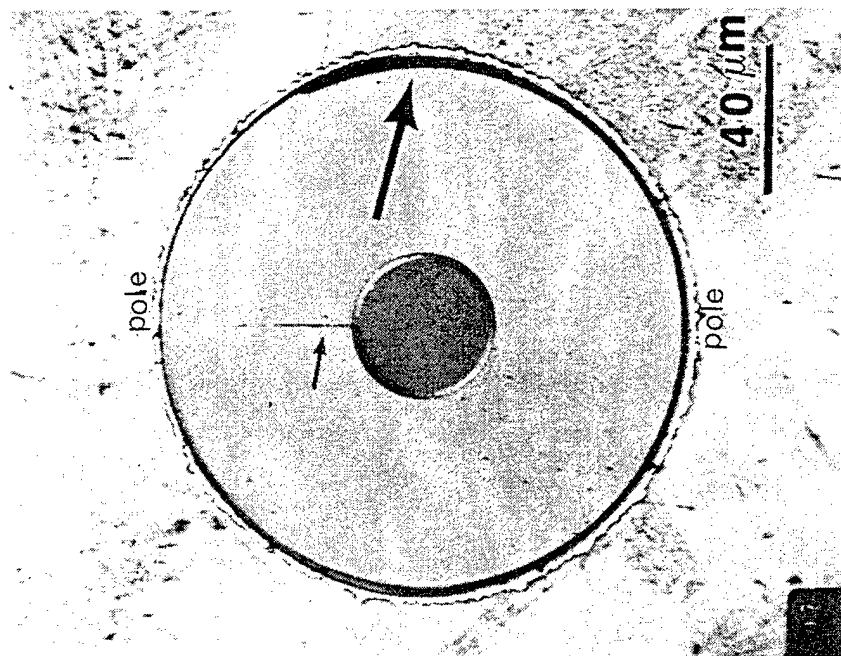


a) 538°C

FIGURE 11. MATRIX PLASTICITY IN THE FORM OF CONCENTRATED SHEAR SLIP BANDS IN $[90]_8$ Ti 15-3/SCS-6 LAMINA UNDER COMPRESSION AT a) 538°C and b) 650°C.



a) 538°C



b) 650°C

FIGURE 12. DEBONDING (LARGE ARROW) AND RADIAL FIBER CRACKING (SMALL ARROW) IN [90]_B Ti 15-3/SCS-6 LAMINA AT a) 538°C AND b) 650°C DURING UP AND DOWN LOADING

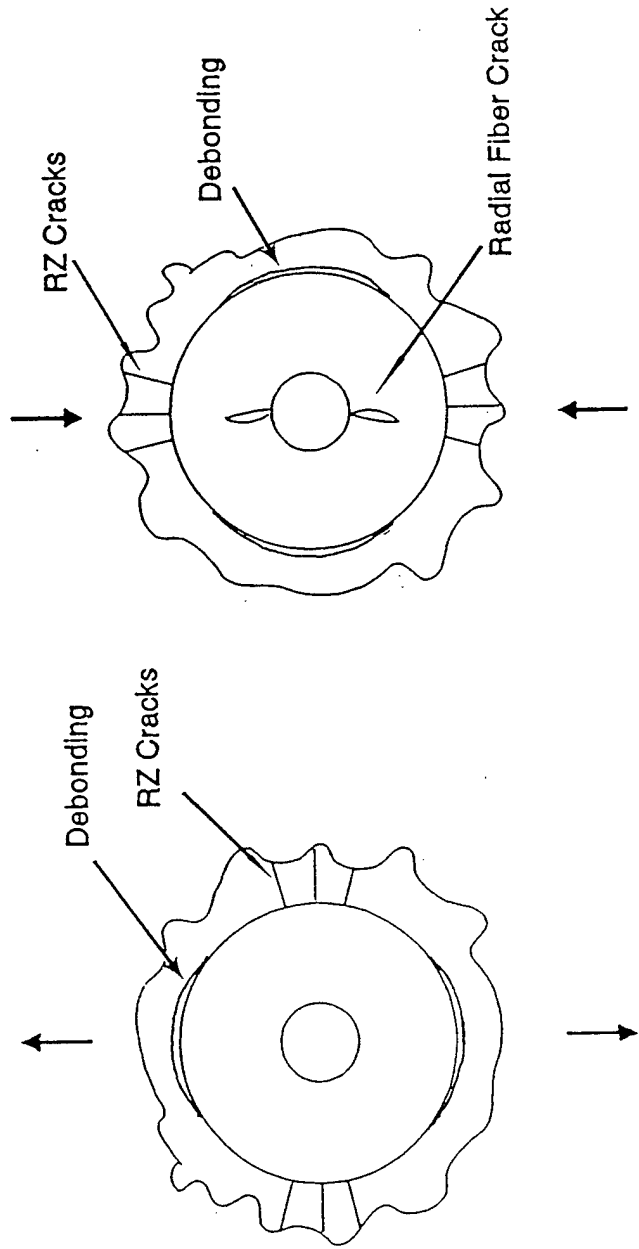
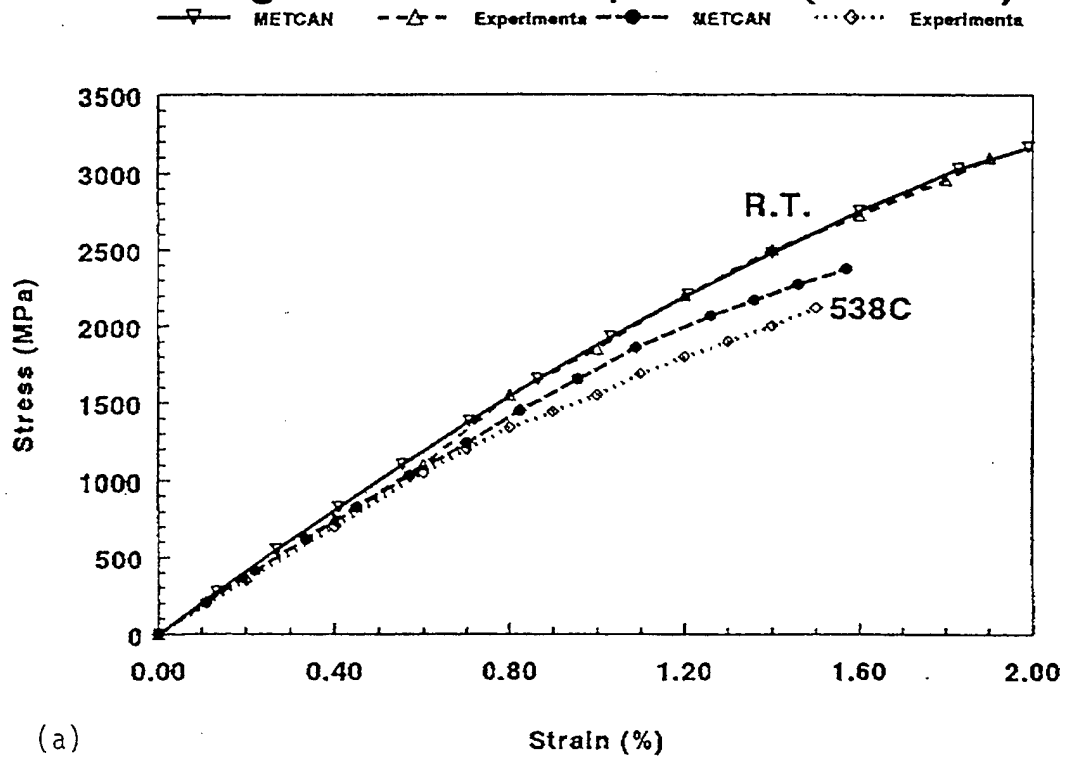


FIGURE 13. ORIENTATION OF DAMAGE (CRACKING) IN TENSION AND COMPRESSION

Longitudinal SCS-6/Ti-15-3 (fvr=0.34)



Transverse SCS-6/Ti-15-3 (fvr=0.34)

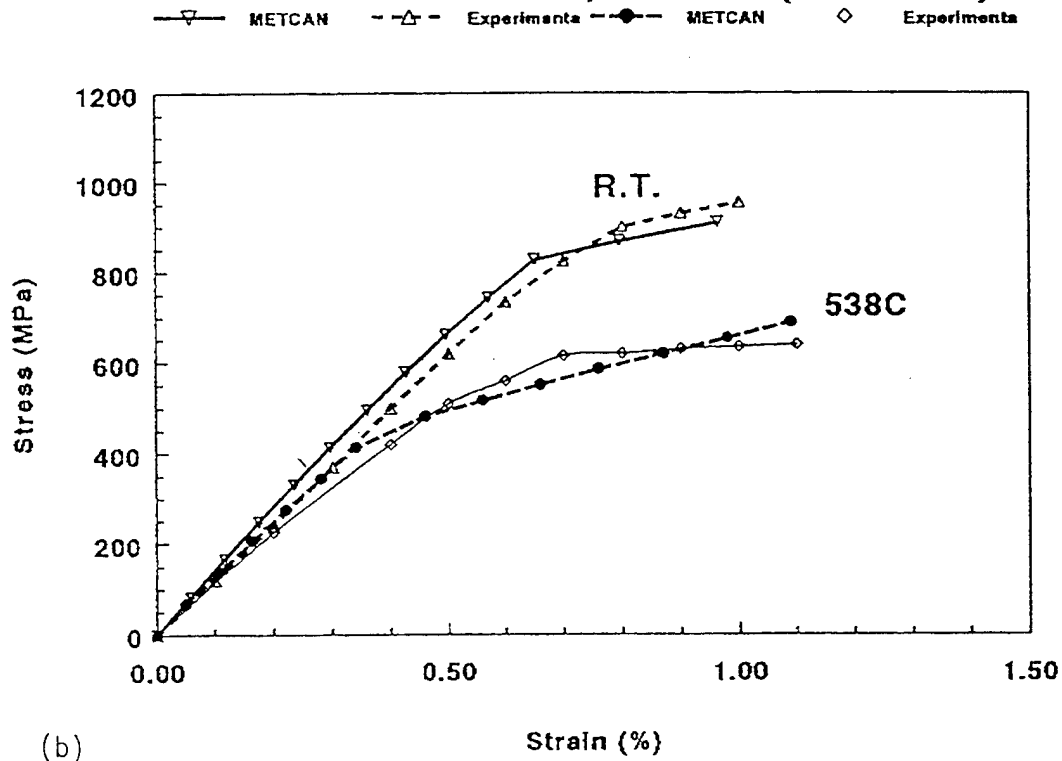


FIGURE 14. METCAN ANALYSIS RESULTS FOR a) $[0]_8$ and b) $[90]_8$ STRESS-STRAIN RESPONSE IN COMPRESSION

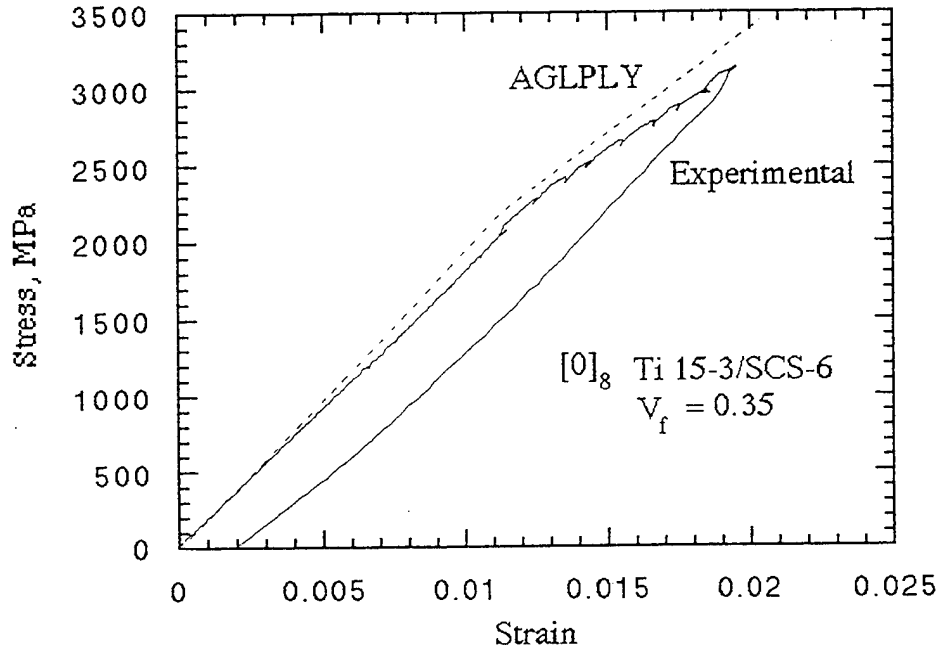


FIGURE 15. AGLPLY ANALYSIS RESULTS FOR $[0]_8$ STRESS-STRAIN RESPONSE IN COMPRESSION

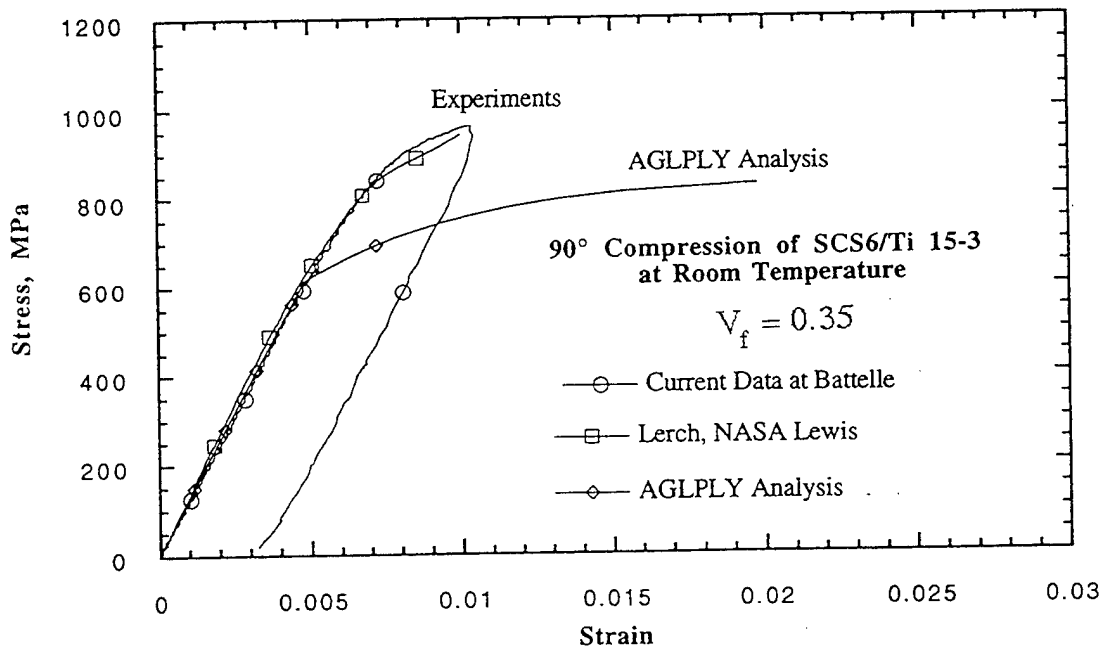


FIGURE 16. AGLPLY ANALYSIS RESULTS FOR $[90]_8$ STRESS-STRAIN RESPONSE IN COMPRESSION

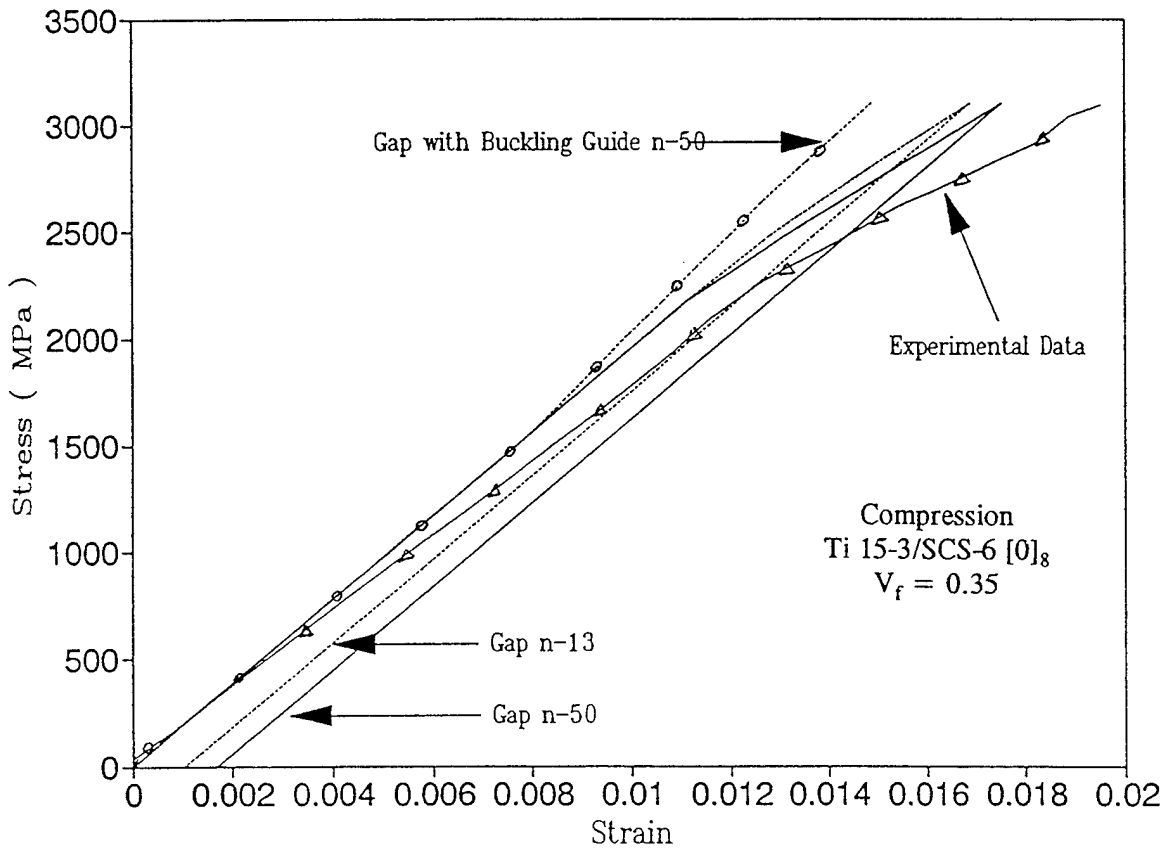


FIGURE 17. BATTELLE'S UNIT CELL COMPUTATIONAL MICROMECHANICS RESULTS FOR $[0]_8$ LAMINA AT RT. VALUES OF n REPRESENT RAMBERG-OSGOOD EXPONENT FOR MATRIX EXPERIMENTAL DATA

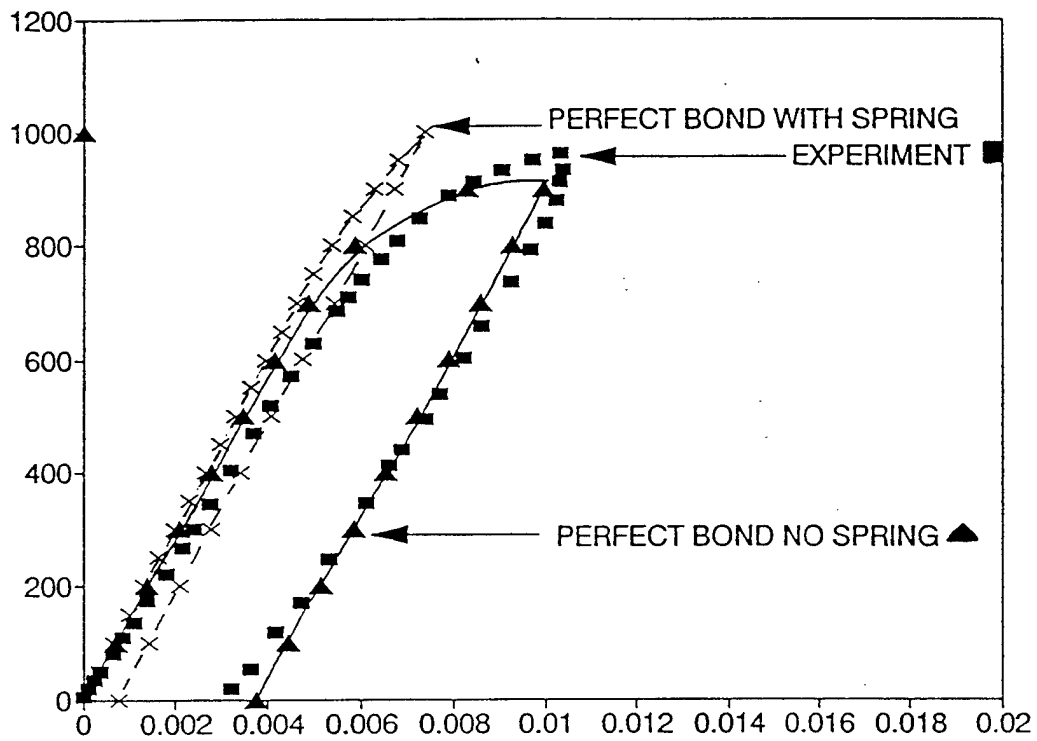
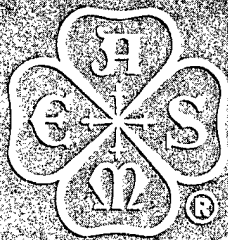
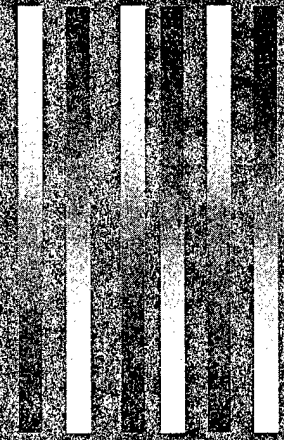


FIGURE 18. BATTELLE'S UNIT CELL COMPUTATIONAL MICROMECHANICS RESULTS FOR $[90]_8$ LAMINA AT RT. LATERAL CONSTRAINT WAS MODELED USING SPRINGS.

MD-Vol. 51

DURABILITY OF COMPOSITE MATERIALS



EDITED BY
R. C. WETHERHOLD

THE NATURE OF COMPRESSIVE FAILURE IN MMC

Golam M. Newaz
Battelle Memorial Institute
Columbus, Ohio

ABSTRACT

Review of previous work on the failure characteristics of $[0]_8$ and $[90]_8$ Ti 15-3/SCS-6 lamina and Beta 21S/SCS-6 subjected to pure compression is undertaken in this article. The inelastic deformation in the $[0]_8$ lamina under compression was controlled primarily by matrix plasticity, although some evidence of fiber-matrix debonding was observed. Failure of the unidirectional specimen in compression was due to fiber buckling in a macroscopic shear zone (the failure plane). The inelastic deformation mechanisms under compression in $[90]_8$ lamina were controlled by radial fiber fracture, matrix plasticity and fiber-matrix debonding. The radial fiber fracture was a new damage mode observed for MMCs. Simple micromechanics models based on specific damage modes are developed and are shown to be effective in predicting the onset of nonlinearity or yield point for the MMCs.

INTRODUCTION

Titanium based metal matrix composites (MMCs) offer excellent potential for high temperature applications which require a combination of high temperature strength, stiffness and toughness. Considerable research in characterizing SiC fiber-reinforced titanium composites have been made to date. A number of relevant studies including that conducted by the author and other coworkers are given in the references [1-14].

The loading mode which has received most attention by researchers in the field is tensile loading. Although, this is certainly the dominant loading mode for the application of the fiber reinforced MMCs, compressive loading in the application of these structural materials is a definite possibility for various components. Compression on one surface is a reality in bending. Furthermore, in the case of reversed fatigue loading, the composite will experience compressive loading in part of the cycle.

It is also anticipated that structural design engineers will require design allowables for tensile, compressive and shear properties. Compressive loading has not received much attention to date for high temperature composites. Past studies on Boron/Aluminum composites concentrated on

their longitudinal compression behavior-[10]; however, their transverse compression behavior was not studied. Understanding of the evolution of damage and failure modes under compressive loading of the MMC at high temperature is seriously lacking. Considerable research is needed to clarify and resolve the micromechanics issues for compressive response. It is also necessary to complement experimental efforts with analytical ones to predict the constitutive response of the MMC under compressive loading since such efforts are not under consideration in any of the major high temperature programs. Furthermore, high temperature data for compression is lacking.

An area that requires considerable attention in the compression response of MMC is the failure behavior of the composites, particularly, the role of fiber and matrix on the overall composite failure. "Failure" is considered to be the onset of extensive inelastic deformation including matrix and fiber-matrix interfacial cracking and fiber fracture. An assessment of failure characteristics of these composites may be essential to define the overall load bearing characteristics of these materials in design applications.

EXPERIMENTAL ASPECTS

SCS-6/Ti 15-3 and SCS-6/Beta 21S composite specimens, namely, $[0]_8$, $[90]_8$ and $[0/90]_{45}$ rectangular test specimens were machined from the unidirectional panels using an electric-discharge machining (EDM) technique, with specimen dimensions of 2.0 mm x 10.2 mm x 104.1 mm. The gage length was 25.4 mm. The specimens were mechanically polished after EDM machining to minimize any damage associated with the machining. All specimens were tested in the as-fabricated condition, i.e., no heat-treatment was performed prior to the testing. Beta 21S/SCS-6 MMCs were tested at RT 483 C, 538 C, 650 C and 815 C. The fiber volume fraction for SCS-6/Ti 15-3 and Beta 21S/SCS-6 was between 0.35 and 0.35-0.40, respectively.

Specimens were gripped using friction grips, and loaded on a servohydraulic testing machine at a strain rate of approximately 0.004/sec. Compression testing was done using a Battelle developed compression fixture which uses buckling guides. The longitudinal strains were measured using an extensometer. Selected specimens were observed under an optical microscope to determine the nature of failure modes.

RESULTS AND DISCUSSION

Failure Mode and Micromechanics Analysis

Mechanical behavior response and the effect of temperature on the onset of nonlinearity (yield strength) for the MMCs are shown in Figures 1-6. Discussion of individual lamina response and failure modes is forwarded next.

Longitudinal Lamina

In earlier studies, it was shown by Newaz and Majumdar [13] that the major deformation in unidirectional MMC under compression was due to matrix plasticity. SCS-6/Ti 15-3 composite was the subject of study in the earlier work. Titanium 15-3 is amenable to slip band formation and it is easy to observe these slip bands in Ti 15-3 than in Beta 21S titanium alloy.

For matrix plasticity as the key deformation mode as shown in Figure 7, the composite compression proportional limit can be estimated to be

$$\sigma_C^L = E_C (\epsilon_O^m + \epsilon_{res}) \quad (1)$$

...ssion behavior was under compressive search is needed to s also necessary to ve response of the in any of the major sion is lacking. se of MMC is the rix on the overall lastic deformation sessment of failure all load bearing

[90]₈ and [0/90]_{4S} electric-discharge x 104.1 mm. The DM machining to tested in the as- Beta 21S/SCS-6 fraction for SCS-

ic testing machine : using a Battelle ns were measured al microscope to

et of nonlinearity l lamina response

or deformation in i 15-3 composite nd formation and

7, the composite

(1)

- ϵ_0^m = matrix yield strain
- ϵ_{res} = residual compressive strain in the loading direction (from cooldown after processing)
- E_c = composite modulus, $E_f V_f + E_m V_m$
- E_f, E_m = fiber and matrix moduli
- V_f, V_m = fiber and matrix volume fraction

For SCS-6/Ti 15-3 composites, $V_f = 0.34$, $E_m = 100$ GPa and $E_f = 400$ GPa, estimated compressive proportional limit is 2324 MPa. Experimental result is 2200 MPa [13]. The matrix yield strain is taken to be $\epsilon_0^m = 0.0075$ and $\epsilon_{res} = 0.0041$ (obtained from finite element calculations). ϵ_{res} can be estimated using analytical model too, e.g., using the Budiansky solution [15] using the concentric cylinder model as described below.

Concentric Cylinder Model:

Axial Residual Stress (p),

$$p/E_m = [\lambda_2/\lambda_1] [E_f/E_c] [V_f \Delta\alpha \Delta T / (1-\nu_m)] \tag{2}$$

where $\lambda_1 = \{1 - (1-E_c/E_f)(1-\nu)/2 - (E_c/E_f)\nu^2\} / (1-\nu^2)$

$$\lambda_2 = 1 - (1-E_c/E_f) / 2$$

$$\nu = \nu_m = \nu_f, c = \text{composite}, m = \text{matrix}, f = \text{fiber}$$

$\Delta\alpha$ = difference in thermal expansion coefficient between fiber and matrix

Radial Residual Stress (q),

$$q/E_m = -[(1-V_f)\Delta\alpha\Delta T]/[2\lambda_1(1-\nu_m)] \tag{3}$$

Transverse Lamina

Deformation mode for transverse lamina is matrix plasticity, fiber-matrix debonding and radial fiber cracking. It has been observed that radial fiber cracking occurs at the onset of nonlinearity during transverse response of the MMC [13]. Based on this mode of failure, proportional limit under compression for transverse lamina is predicted and matches well with experimental results.

For the deformation mode of fiber radial cracking as shown in Figure 8, local fiber-matrix stress is given by:

$$\sigma_f = S \cdot \sigma_c^T \tag{4}$$

$$S = [1 - V_f(1 - E_m/E_f)] / [1 - (4V_f/\pi)^{1/2}(1 - E_m/E_f)] \tag{5}$$

$$V_f = 0.34, E_m = 100 \text{ GPa}, E_f = 400 \text{ GPa}$$

$$S = 1.45$$

$\sigma_f + \sigma_{res} = \sigma_{fu}^T, \sigma_{fu}^T \approx$ fiber transverse compressive strength, 1200 MPa (experimental value obtained by Elridge [16])

$$\sigma_{\text{res}} \approx 200 \text{ MPa (FEA or analytical)}$$
$$\sigma_t = 1000 \text{ MPa}$$
$$\sigma_C^T = 1000/1.45 = 690 \text{ MPa}$$

This value compares very well with a value of $\sigma_C^T = 700 \text{ MPa}$ obtained experimentally by Newaz and Majumdar [13].

Macroscopic Fracture Characteristics

Extensive inelastic deformation may lead to "failure" of the composite. continued loading may result in final loss in load carrying capability and fracture of the MMC. In this section, we briefly discuss macroscopic fracture characteristics of the MMC.

Longitudinal Lamina

The failure due to fiber buckling in an unrestrained test is shown in Figure 9. The fibers break in a shear plane within the gage section. This failure is indicative of a buckling instability due to compressive load. Microstructural evaluation was only conducted for Ti 15-3 system. Fiber-matrix debonding is also evident at higher strain levels within the ply [11-13].

Transverse Lamina

Optical photomicrographs of specimens polished after testing revealed the nature of deformation characteristics under compressive loading quite clearly. The initial deformation mechanism under monotonic compressive loading is found to be matrix plasticity along the loading axis between fibers as shown in Figure 10 for a specimen tested at room temperature. There is radial fiber cracking and fiber-matrix debonding as well.

CONCLUSIONS

The failure characteristics in longitudinal MMC lamina is strongly influenced by matrix plasticity whereas it is strongly influenced by a combination of inelastic events such as fiber-matrix debonding, matrix plasticity and fiber radial fracture for the transverse MMC lamina. Simple micromechanics models which relate to these inelastic events can accurately predict the onset of "failure" or extensive nonlinearity for the MMCs.

ACKNOWLEDGEMENT

This research effort was supported by AFOSR, Dr. Walter Jones, Program Monitor. The author acknowledges various discussions with him and Dr. Theodore Nicholas of AFWAL during the course of the program.

REFERENCES

1. Lerch, B. A. and Saltsman, J. F., "Tensile Deformation Damage in SiC Reinforced Ti-15V-3Cr-3Al-3Sn", NASA Technical Memorandum 103620, April, 1991.
2. Sun, C. T., "Modeling Continuous Fiber Metal Matrix Composite as an Orthotropic Elastic-Plastic Material", ASTM STP 1032, 1989, pp. 148-160.

Newaz, G. M., Majumdar, B. S. and Brust, F. "Thermal Cycling Response of Quasi-Isotropic Metal-Matrix Composites", ASME J. of Engg. Materials and Technology, April, 1992, pp. 156-161.

4. Majumdar, B. S. and Newaz, G. M., "Thermomechanical Fatigue of a Quasi-Isotropic Metal Matrix Composite", ASTM STP 1110, 1991, pp. 732-752.
5. Johnson, W. S., Lubowinski, S. J. and Highsmith, A. L., "Mechanical Characterization of Unnotched SCS-6/Ti-15-3 Metal Matrix Composites at Room Temperature", ASTM STP 1080, pp. 193-218, 1990.
6. Nimmer, R. P., Bankert, R. J., Russell, E. S., Smith, G. A. and Wright, K. P., "Micromechanical Modeling of Fiber/ Matrix Interface Effects in Transversely Loaded SiC/Ti-6-4 Metal Matrix Composites Technology and Research, Vol. 13, #1, 1991, pp. 3-13.
7. Majumdar, B. S. and Newaz, G. M., "Inelastic Deformation in Metal Matrix Composites: Plasticity and Damage Mechanisms", Philosophical Magazine, London, 1992, Vol. 66, #2, pp 187-212.
8. Gunawardena, S. R., Jansson, S. and Leckie, F. A., "Transverse Ductilities of Metal Matrix Composites", AD-22, ASME Winter Annual Meeting, Atlanta, December, 1991, pp. 23-30.
9. Newaz, G. M. and Majumdar, B. S., "Deformation and Failure Mechanisms in MMC", AD-22, ASME Winter Annual Meeting, Atlanta, 1991, pp. 55-66.
10. Lamothe, R. M. and Nunes, J., "Evaluation of Fixturing for Compression Testing of Metal Matrix and Polymer Matrix Composites", ASTM STP 808, R. Chait and R. Paprino, Eds., 1983, pp. 241-253.
11. Newaz, G. M. and Majumdar, B. S., "Failure Modes in Transverse MMC Lamina Under Compression" J. of Materials Science & Letters, UK, December, 1992.
12. Newaz, G. M. and Majumdar, B. S., "Inelastic Deformation Mechanisms in a Transverse MMC Lamina Under Compression," AD-Vol. 27, Fracture and Damage, ASME Winter Annual Meeting, Anaheim, 1992, pp. 77-84.
13. Newaz, G. M. and Majumdar, B. S., "Inelastic Deformation in MMC Under Compression," NASA Contractor Report #191170, HITEMP, Cleveland, 1993.
14. Newaz, G. M., "Constitutive Response and Deformation Mechanisms in Unidirectional MMC Under Compression," Presented at the ASTM Symposium on 12th Composite Materials Testing and Design, Montreal, May, 1994.
15. Budiansky, B., Hutchinson, J. W. and Evans, A. G., "Mechanics of Physics and Solids," Vol. 34, 1986, p. 167.
16. Eldridge, J. I., Wienen, J. P., Davison, T. S. and Pindera, M-J., "Transverse Strength of SCS-6 Silicon Carbide Fibers," J. of American Ceramic Society, Vol. 76 (#12), 1993, pp. 3151-54.

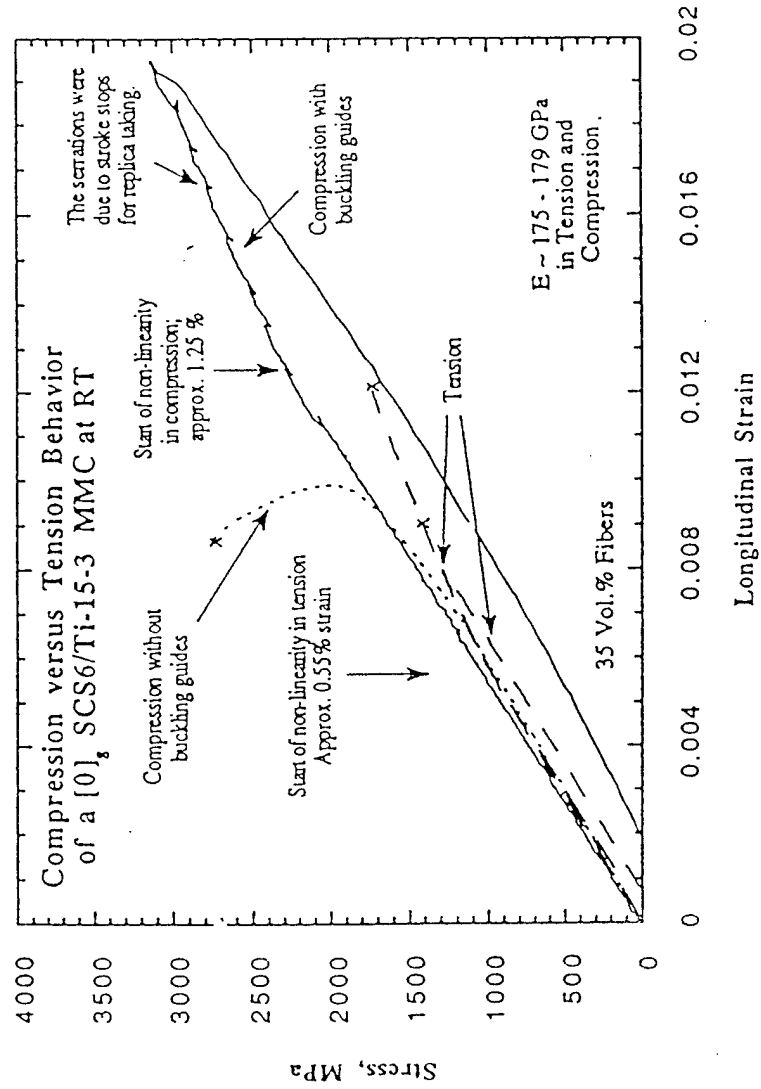


FIGURE 1. COMPRESSION RESPONSE OF [0]_s TI 15-3/SCS-6 COMPOSITE SHOWING THE DIFFERENCE WITH AND WITHOUT BUCKLING GUIDES. RESULTS ARE COMPARED WITH TENSION RESPONSE AS WELL.

Longitudinal Strain

FIGURE 1. COMPRESSION RESPONSE OF [0]_g TI 15-3/SCS-6 COMPOSITE SHOWING THE DIFFERENCE WITH AND WITHOUT BUCKLING GUIDES. RESULTS ARE COMPARED WITH TENSION RESPONSE AS WELL.

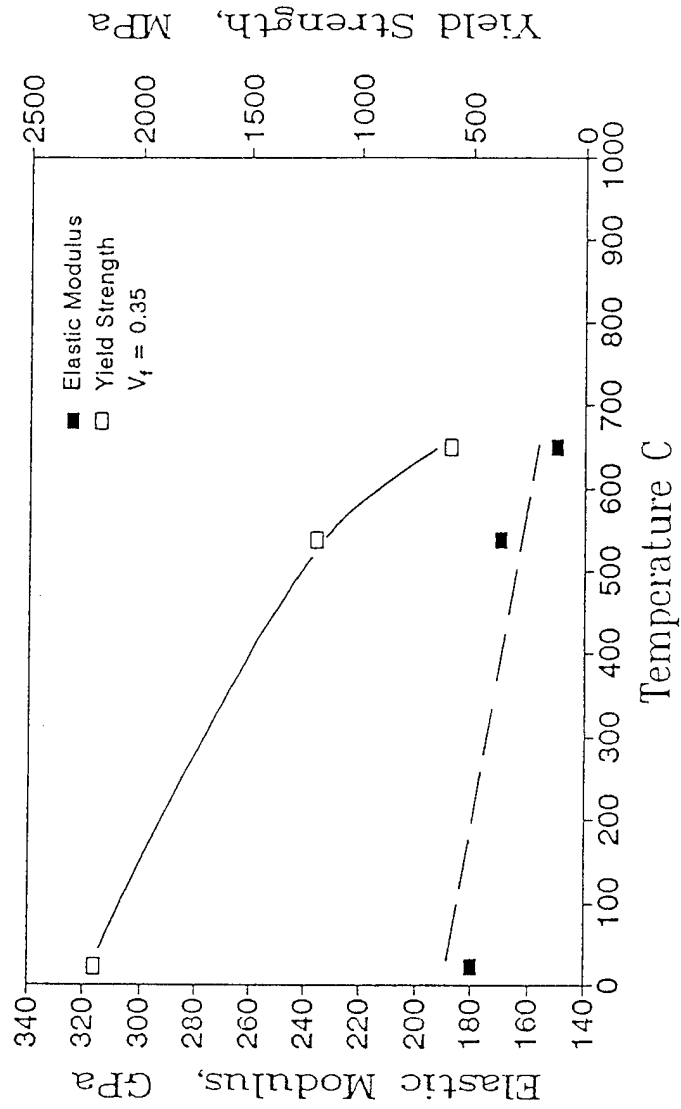


FIGURE 2. DEGRADATION OF MODULUS AND YIELD STRENGTH AS A FUNCTION OF TEMPERATURE IN [0]_g TI 15-3/SCS-6 COMPOSITE IN COMPRESSION.

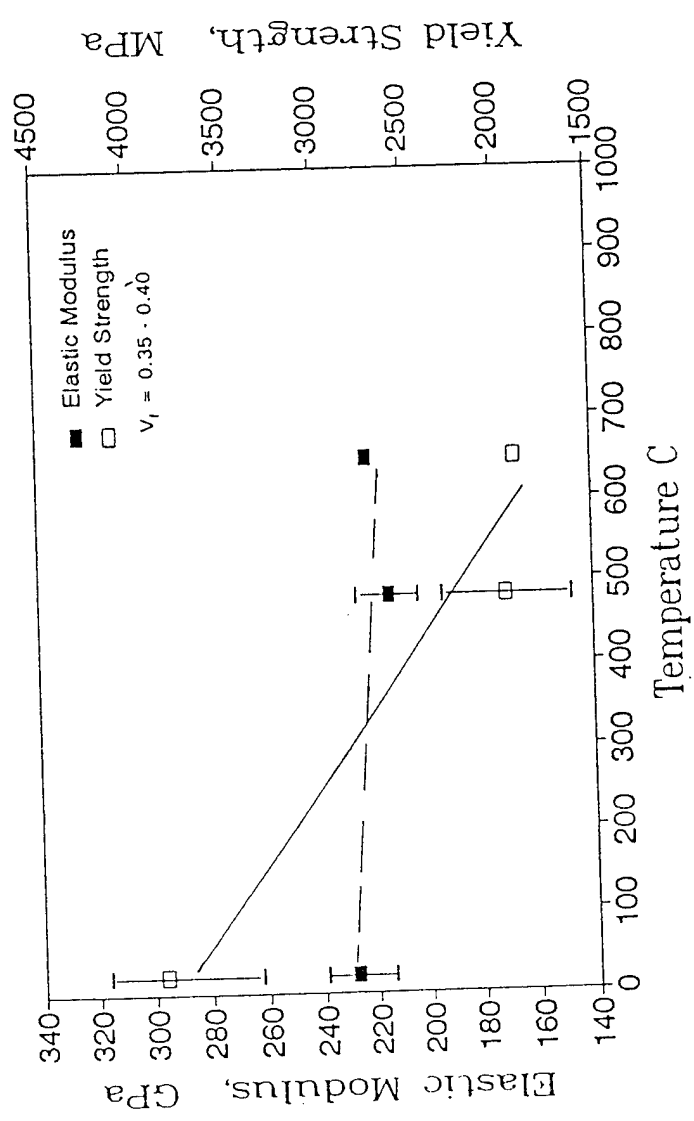


FIGURE 3. DEGRADATION OF MODULUS AND YIELD STRENGTH AS A FUNCTION OF TEMPERATURE IN [0]₈ BETA 21S/SCS-6 COMPOSITE IN COMPRESSION.

FIGURE 3. DEGRADATION OF MODULUS AND YIELD STRENGTH AS A FUNCTION OF TEMPERATURE IN $[0]_8$ BETA 21S/SCS-6 COMPOSITE IN COMPRESSION.

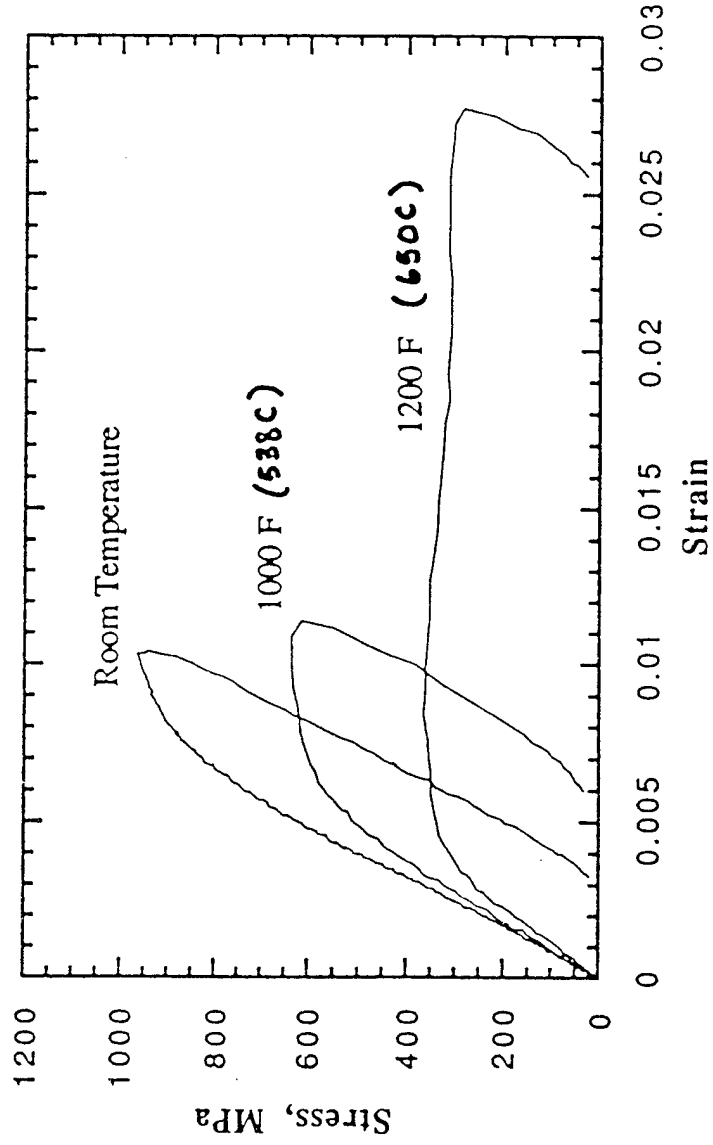


FIGURE 4. COMPRESSION RESPONSE OF $[90]_8$ TI 15-3/SCS-6 COMPOSITE.

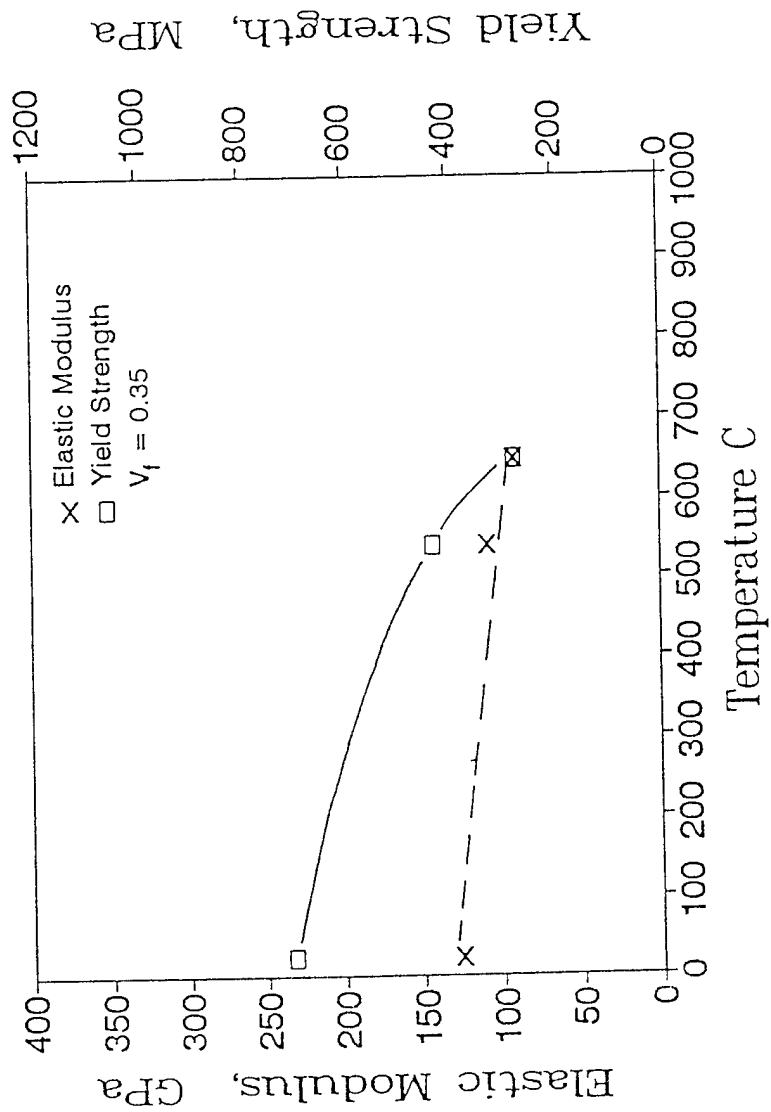


FIGURE 5. DEGRADATION OF MODULUS AND YIELD STRENGTH AS A FUNCTION OF TEMPERATURE IN [90]₈ TI 15-3/SCS-6 COMPOSITE IN COMPRESSION.

FIGURE 5. DEGRADATION OF MODULUS AND YIELD STRENGTH AS A FUNCTION OF TEMPERATURE IN [90]₈ TI 15-3/SCS-6 COMPOSITE IN COMPRESSION.

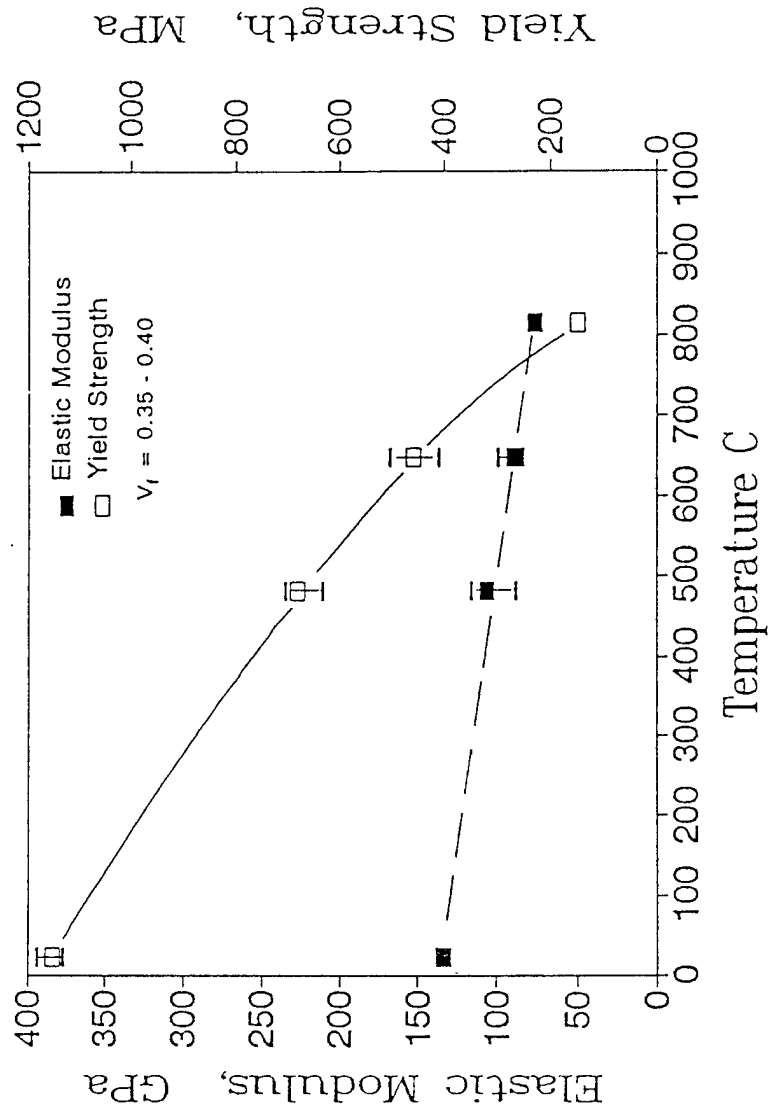


FIGURE 6. DEGRADATION OF MODULUS AND YIELD STRENGTH AS A FUNCTION OF TEMPERATURE IN [90]₈ BETA 21S/SCS-6 COMPOSITE IN COMPRESSION.

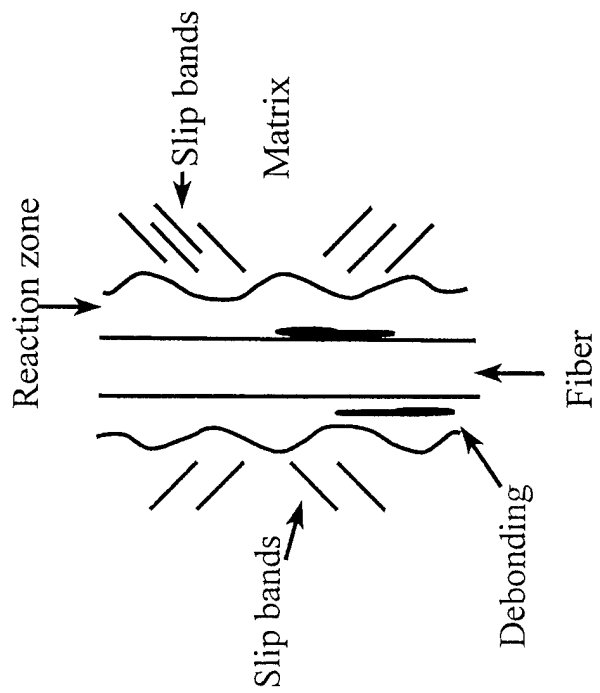


FIGURE 7. MATRIX PLASTICITY AS A DOMINANT DEFORMATION MODE IN UNIDIRECTIONAL MMC.

FIGURE 7. MATRIX PLASTICITY AS A DOMINANT DEFORMATION MODE IN UNIDIRECTIONAL MMC.

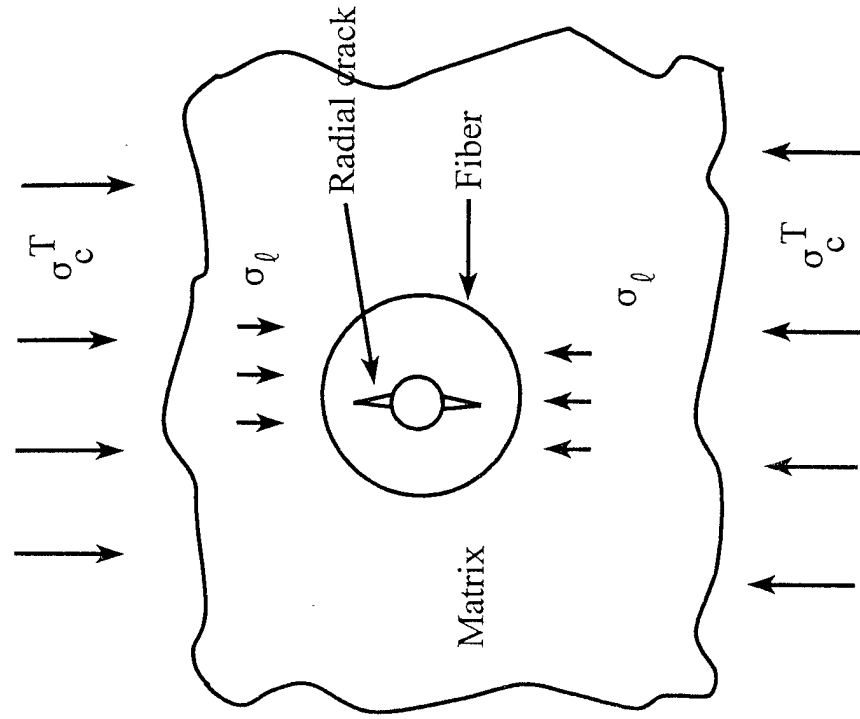


FIGURE 8. FIBER RADIAL CRACKING AS A MAJOR FAILURE MODE IN SCS 6 REINFORCED TRANSVERSE MMC.

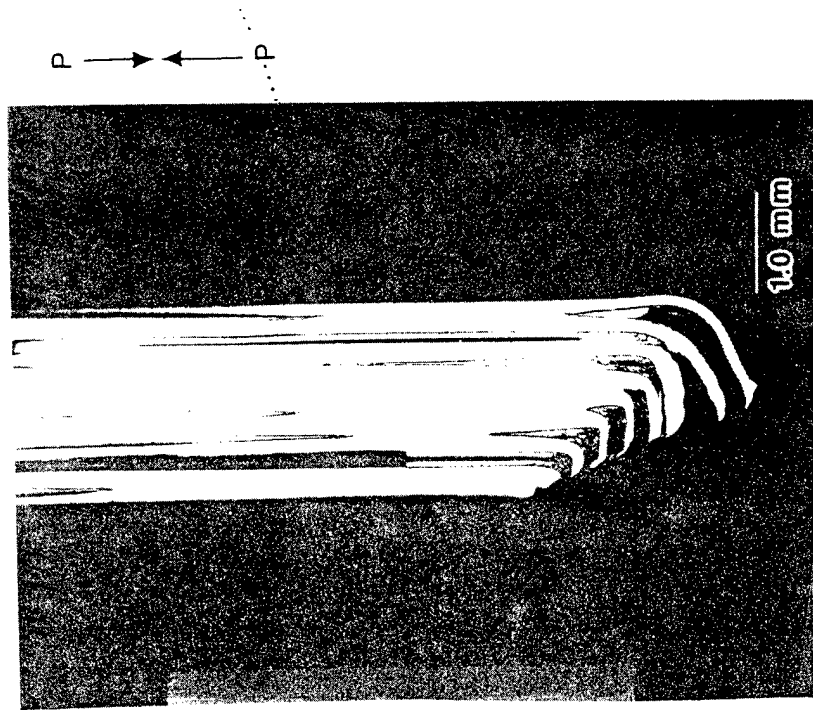


FIGURE 9. FIBER BUCKLING IN $[0]_8$ LAMINA IN COMPRESSION AT RT.



FIGURE 9. FIBER BUCKLING IN $[0]_8$ LAMINA IN COMPRESSION AT RT.

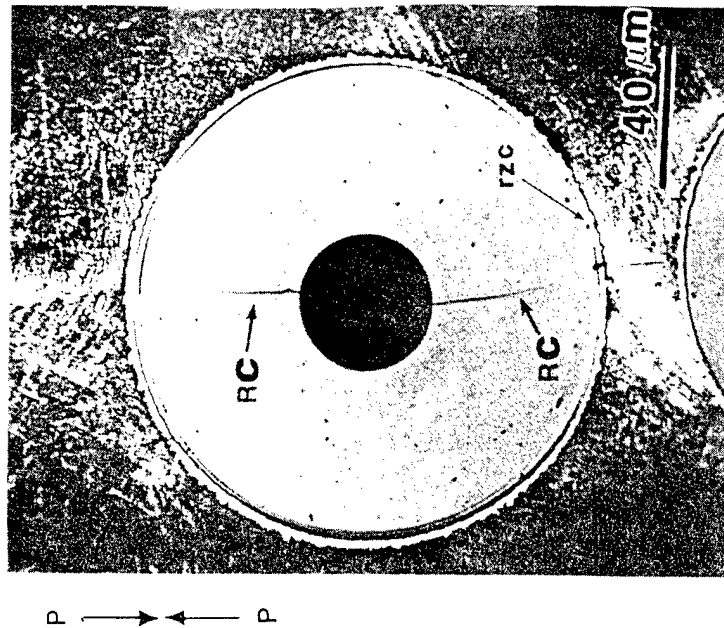


FIGURE 10. RADIAL CRACKS IN SCS-6 FIBER IN A $[90]_8$ Ti 15-3/SCS-6, LAMINA UNDER COMPRESSION AT ROOM TEMPERATURE. LOADING IS UP AND DOWN.

DAMAGE INITIATION AND FAILURE MODES IN A UNIDIRECTIONAL MMC WITH A HOLE UNDER TENSION AND COMPRESSION

G. M. Newaz and M. Krishnappa
Wayne State University, Detroit, MI 48202

and

N. Bonora
University of Cassino, Cassino, Italy

ABSTRACT

In this investigation, unidirectional eight-ply Ti 15-3/SCS-6 composites with center holes were subjected to monotonic compression and compression-compression fatigue loading at room temperature. Optical microscopy was used to evaluate the initiation and growth of the cracks and to determine their angular orientation around the hole in the specimen. Under fatigue loading, it was found that the cracks initiated at 65-72 degrees from the vertical axis. The Hencky-Von Mises failure criterion, an octahedral shear stress criterion, was found to be successful in predicting the preferred initiation sites for the major failure cracks. Fatigue crack initiation appeared to be controlled primarily by shear stress induced reversed inelastic deformation of the matrix in the hole region. Also, under monotonic loading, cracks initiated at 65-72 degrees from the vertical axis. Under both compression and compression-compression fatigue loading, shear induced damage is observed. These failure modes were compared with those observed under monotonic tension and tension-tension fatigue loading and are rationalized.

INTRODUCTION

Applications of high temperature composites such as metal-matrix and intermetallic-matrix composites (MMCs and IMCs) are receiving much attention. These composites offer both weight reduction and improved properties at high temperatures. Extensive characterization is now underway to evaluate the capabilities of metal-matrix and intermetallic composites for applications involving both thermal and mechanical loads.

A major consideration in aerospace applications is damage tolerance. For these material systems, there are no acceptable damage tolerance methodologies available today. Much of the difficulty stems from the fact that very little is known about the failure characteristics of these new classes of materials and whatever information is available tends to show the very complex nature of damage evolution in these materials. Although a few pioneering studies by Waddoups *et al.* [1] and Nuismer and Whitney [2] have shed light on fracture characteristics of composites with holes, they are limited to static loads and are specific to polymeric composites (PMCs). The failure modes in various types of composites can be quite different. As a result, generalized conclusions about fracture characteristics of MMCs based on the information available for PMCs can not be made.

For MMCs a limited number of fatigue studies with holes have been conducted. The fatigue failure of unidirectional alumina fiber-reinforced aluminium (Al/FP alumina) with circular holes was modeled by Tsangarakis [3]. Prediction of notch endurance limit

was achieved with a reasonable accuracy using a modification of the Whitney and Nuismer model [4]. In a subsequent study, Tsangarakis studied the sequence of fatigue damage accumulation in Al/SiC composites [5]. However, these studies did not address the issues of fracture morphology and preferred crack initiation sites. Recently, Harmon and co-workers [6,7] studied the differences in failure modes of Al/Boron, Ti 15-3/SCS-6 and Ti 6-4 composites containing center hole. Titanium alloy based MMCs showed distinctively different failure modes compared with Al/boron MMCs. However, the microscopic mechanism of crack initiation was not adequately addressed. In a related study, Newaz et al [8] investigated the initiation and growth of cracks around holes in unidirectional titanium MMCs subjected to monotonic and fatigue loadings. The failure modes observed for monotonic tension and tension-tension fatigue were quite different. In the former case, failure was due to normal stress and fiber failure in a plane perpendicular to the applied loading direction (Fig. 1). In tension-tension fatigue, the damage initiation occurred at 65-72 degrees from the pole with four symmetric cracks (Fig. 2). These cracks were determined to initiate in shear and at some distance away from the hole continued to grow perpendicular to the loading direction.

The purpose of the study was to evaluate the nature of fatigue crack initiation and growth from circular holes in unidirectional Ti 15-3/SCS-6 composites at room temperature under compressive loading. The primary goal was to determine the preferred crack initiation sites under monotonic and fatigue loading. Also, the failure modes under compression were compared with the failure modes observed under tension loading [8].

MATERIALS AND EXPERIMENTAL PROGRAM

The material chosen for this investigation was a unidirectional eight-ply Ti 15-3/SCS-6 composite. The reinforcing phase (approximately 40 volume-percent) was continuous 140 μm diameter SiC fibers, commercially designated as SCS-6. The matrix material was a beta-phase Ti-15V-3Al-3Sn-3Cr (weight percent) alloy. The composite was fabricated by Avco Speciality materials, Textron by hot isostatically pressing (HIP-ing) alternate layers of fibers and thin foils of Ti 15-3, with ribbons of Mo used to fibers in alignment.

Table 1. Average properties of Ti 15-3/SCS-6 $[0]_8$ composite at room temperature

Moduli (Gpa)	$E_L = 207$	$E_T = 124.2$	$G_{LT} = 55.2$
Possion's ratio	$\nu_{LT} = 0.24$	$\nu_{TL} = 0.15$	
Strengths (MPa)	$F_L = 1587$	$F_T = 256$	$F_{TL} = 289.8$

Fiber volume fraction = 0.38

The thickness of each ply was approximately 0.19 mm. The average room temperature properties of the composite are listed in Table 1. The strength values reported in the table are for a tension case. Compression strength values are taken to be compression yield values and are considered to be similar to the tension strength values

given in the Table above. F_L value of 1587 MPa is a lower bound under compression. Since slip bands are observed early in compression under transverse loading[9], F_T values may be taken as a lower bound in compression as well. Based on these considerations, the properties given in Table 1 will be used both for tension and compression cases.

The specimen dimensions are 152.4 x 19.0 x 1.55 mm, with the tensile axis oriented along the fiber direction (0 degree MMC). The specimens are machined with a diamond wheel using a 50/50 mix of water and glycol during the cutting operation. A center hole of 9.53 mm diameter was drilled in each specimen using electric discharge machining (EDM). The surfaces of the holes are subsequently polished using emery paper.

Fatigue testing was conducted at a frequency of 2 Hz and an R -ratio of 0.1 and -0.1 on a servo-hydraulic test system. Specimens were tested at a stress range of 710 MPa. A few samples were tested in compression to failure under monotonic loading to determine the notch strength and failure mode. The notch strength was approximately 1000 MPa. All testing was performed at room temperature.

Optical microscopy was conducted using a number of specimens to determine the nature and location of crack initiation under compression.

ANALYTICAL CONSIDERATIONS

Stresses around a hole in a unidirectional composite

For the case of an uniaxially loaded plate in which the loading direction coincides with the fiber direction (Fig. 1), the circumferential stress at the edge of the opening is given by the following equation [10]:

$$\sigma_{\theta L} = \left\{ \frac{(1+\gamma_1)(1+\gamma_2)(1+\gamma_1+\gamma_2-\gamma_1\gamma_2-2\cos 2\theta)}{(1+\gamma_1^2-2\gamma_1\cos 2\theta)(1+\gamma_2^2-2\gamma_2\cos 2\theta)} \right\} \sigma_L \quad (1)$$

where

$$\gamma_1 = \frac{\left[\left(\frac{E_T}{2G_{LT}} - \nu_{TL} \right) + \sqrt{\left(\frac{E_T}{2G_{LT}} - \nu_{TL} \right)^2 - \frac{E_T}{E_L}} \right]^{1/2}}{\left[\left(\frac{E_T}{2G_{LT}} - \nu_{TL} \right) + \sqrt{\left(\frac{E_T}{2G_{LT}} - \nu_{TL} \right)^2 - \frac{E_T}{E_L}} \right]^{1/2}} - 1 \quad (2)$$

$$\gamma_2 = \frac{\left[\left(\frac{E_T}{2G_{LT}} - \nu_{TL} \right) + \sqrt{\left(\left(\frac{E_T}{2G_{LT}} - \nu_{TL} \right)^2 - \frac{E_T}{E_L} \right)} \right]^{1/2} - 1}{\left[\left(\frac{E_T}{2G_{LT}} - \nu_{TL} \right) + \sqrt{\left(\left(\frac{E_T}{2G_{LT}} - \nu_{TL} \right)^2 - \frac{E_T}{E_L} \right)} \right]^{1/2} + 1}$$

and E_L the modulus of elasticity in the fiber direction (x or L), E_T is the modulus of elasticity in the transverse direction (y or T), G_{LT} is the in-plane shear modulus, and ν_{TL} is the poisson's ratio giving the transverse strain caused by the stress in the L direction. The stresses σ_{xL} , σ_{yL} and σ_{xyL} associated with the principal axes of the plate are

$$\sigma_{xL} = \sigma_{\theta L} \sin^2 \theta, \quad \sigma_{yL} = \sigma_{\theta L} \cos^2 \theta, \quad \sigma_{xyL} = -\sigma_{\theta L} \sin \theta \cos \theta \quad (3)$$

In isotropic homogeneous plates, yielding ahead of a hole is dominated by the principal stress in the loading direction. Thus the shear and distortional energy theories predict that yielding will occur at 90 degrees to the pole ($\theta = 90$, see Fig. 3). In orthotropic and anisotropic plates containing openings, the yield locations are changed because of interaction of various stress components. Although a comprehensive flow rule for MMCs has yet to evolve, we shall for the time being rely on the Hencky-Von Mises distortion energy theory [10], for predicting the preferred yield location in the vicinity of a hole in a unidirectional composite. According to this theory, the yield criterion for a general orthotropic plate is given by

$$1 = \left(\frac{\sigma_x}{F_x} \right)^2 + \left(\frac{\sigma_y}{F_y} \right)^2 + \left(\frac{\sigma_{xy}}{F_{xy}} \right)^2 - K \frac{\sigma_x \sigma_y}{F_x F_y}, \quad (4)$$

where

$$K = \frac{E_x(1 + \nu_{yx}) + E_y(1 + \nu_{xy})}{2\sqrt{E_x E_y(1 + \nu_{xy})(1 + \nu_{yx})}} \quad (5)$$

F_x , F_y and F_{xy} are the strengths and σ_x , σ_y and σ_{xy} are applied (or induced) stresses associated with directions x and y. For the case of a uniaxially loaded plate (with a hole) in which the load directions coincides with the fiber direction, substitution of eqns.(1) and (3) into eqn. (4) provides the following equation governing yielding along the hole periphery:

$$1 = \left\{ \frac{\sin^4 \theta}{F^2_L} + \frac{\cos^4 \theta}{F^2_T} + \frac{\sin^2 \theta \cos^2 \theta}{F^2_{LT}} - K^* \left(\frac{\sin^2 \theta \cos^2 \theta}{F_L F_T} \right) \right\} \sigma_{\theta L}^2, \quad (6)$$

where $\sigma_{\theta L}$ is given by eq. (1), K^* is now

$$K^* = \frac{E_L(1+\nu_{TL}) + E_T(1+\nu_{LT})}{2\sqrt{E_L E_T}(1+\nu_{LT})(1+\nu_{TL})} \quad (7)$$

and F_L , F_T and F_{LT} are material strength properties associated with directions L and T. Using eqn. (1), $\sigma_{\theta L}$ can be expressed in terms of externally applied stress σ_L , so that yielding condition around the periphery of the hole in a unidirectional composite, loaded in the fiber direction, is given by

$$\beta = 1,$$

where

$$\beta = \left\{ \frac{\sin^4 \theta}{F^2_L} + \frac{\cos^4 \theta}{F^2_T} + \frac{\sin^2 \theta \cos^2 \theta}{F^2_{LT}} - K^* \left(\frac{\sin^2 \theta \cos^2 \theta}{F_L F_T} \right) \right\}^* \left\{ \frac{(1+\gamma_1)(1+\gamma_2)(1+\gamma_1+\gamma_2-\gamma_1\gamma_2-2\cos 2\theta)}{(1+\gamma_1^2-2\gamma_1\cos 2\theta)(1+\gamma_2^2-2\gamma_2\cos 2\theta)} \right\}^2 \sigma_L^2 \quad (8)$$

$\beta < 1$ implies no yielding.

In the discussion that follows, the value of β along the hole periphery will be used for rationalizing the preferred locations for fatigue cracks. It is known that stress components attenuate rather rapidly for $r > a$, so that even if β becomes greater than 1 at the hole periphery, it may become less than unity within, say, one fiber distance from the hole periphery. Since the emphasis in this paper is on qualitative aspects of yielding, we have avoided more detailed analysis of the average stress components. However, the relative magnitudes of β (even those greater than unity) for various θ are expected to provide relative estimates of the magnitude of yielding along the hole periphery.

RESULTS AND DISCUSSION

In the monotonic tension mode, the crack initiation and failure is due to fiber fracture. The initiation site is at 90 degrees from the pole as shown in Figure 1. The failure of the specimen is dominated by fiber fracture mechanism. In Reference 8, it has been shown that although there can be shear induced plastic deformation at the 65-72 angles from the pole at four points along the periphery of the hole, fiber fractures at the 90 degree locations control the overall fracture process of the composite.

In tension-tension fatigue, the crack initiation sites are found to occur at 65-72 degrees from the pole, in four symmetric locations as shown in Figure 2. It was

determined in a previous study by Newaz et.al. [8] that fatigue crack initiation was confined to the matrix. Also, reversed inelastic deformation was attributed to the initiation of the fatigue cracks. Based on the fact that local yielding was most favored at these angles, it was determined that initiation of cracks at these sites was most likely to occur.

In order to obtain an understanding of why fatigue cracks initiate at angles between 65 to 72 degrees from the pole, we have analyzed the results in terms of the location for matrix yielding. The reason for adopting this approach include: (1) fatigue cracks in the MMC were totally limited to the matrix; (2) past work [11,12] on MMCs suggests that for fatigue lives in the 10,000-100,000 cycle range, fatigue failures are largely controlled by matrix fatigue failure; and (3) in the case of homogeneous metals, fatigue life is determined by the inelastic strain range. Thus, the rationale is that fatigue cracks would likely initiate at those locations along the hole periphery which experienced the maximum inelastic strain range.

The three components of stress for the Ti 15-3/SCS-6 MMC, along the hole periphery, are plotted in Fig. 4; the stresses have been normalized with respect to the applied stress. As expected, the maximum principal stress occurs at 90 degrees to the pole, similar to the case of homogeneous metals. However, unlike the case of homogeneous metals, where yielding also occurs at the same 90 degree location, the yielding location for the MMC is changed as discussed below.

Figure 4 shows that the shear stress σ_{xy} has a broad maxima in the 62-72 degree range where fatigue cracks were generally found to initiate for the MMC. This suggests that this shear stress component likely had an influence on fatigue crack initiation. Also plotted in Fig. 4 is the value of β according to the Hencky-Von Mises (H-VM) theory [eq. (8)]. The applied strains were taken as 710MPa. The H-VM criterion shows a strong peak at θ of approximately 68 degrees, indicating that yielding should occur at that angle at the hole periphery. This location for yielding agrees very well with the observed location for major fatigue cracks. During the calculation of β using eq. (8) for eq. (4), it was found that the shear stress term (σ_{xy} / F_{LT}) had the strongest contribution, due primarily to the low intra-laminar shear strength (F_{LT}) of the unidirectional composite at yielding. The σ_{xy} contribution was followed by the σ_y and then the σ_x term. Thus, these calculations, and agreement with observed fatigue crack nucleation location, imply that the fatigue crack initiation from the hole most likely occurs by inelastic deformation of the composite, and is dominated by the amplitude of intra-laminar shear stress (σ_{xy}), parallel to the fiber direction. Although not shown here, recent studies [13-15] indicate that failure is dominated by plastic deformation of the matrix material. For loading perpendicular to the fiber direction, plasticity also dominates at strains above 0.6 percent. The dominance of matrix plasticity suggests that in the case of current MMC with a hole, fatigue crack nucleation is controlled by the amplitude of plastic strain of the matrix material, similar to what occurs in homogeneous metals. Indeed, we did observe significant slip band activity in the matrix of the MMC in the 60-75 degree range [8].

In compression, the stresses around the periphery are compression in nature. As a result, likely crack initiation sites are controlled by shear due to compression. The description of the stress field and severity given by Equations 1-3 around the hole is

altered through the change in sign only. Therefore, the maximum severity around the hole will be given by the same beta parameter in Equation 8. Under monotonic loading, the initiation sites are oriented at 65-72 degrees from the loading axis. The subsequent failure of the specimen is controlled by fiber-matrix interfacial splitting parallel to the loading direction as shown in Fig. 5 and Fig. 6. In the absence of any tension components, we anticipate that the same points around the periphery of the hole will be affected under compression-compression fatigue. This was also confirmed for the MMC specimens tested under compression-compression fatigue.

CONCLUSIONS

The following conclusions can be drawn from the current investigation.

1. Crack initiation from a central hole in unidirectional MMC takes place at the same angular orientation in tension-tension fatigue and in monotonic compression and compression-compression fatigue. For the SCS-6/Ti 15-3 composite with fiber volume fraction of 0.38 this orientation is between 65-72 degrees from the loading axis. The initiation locations are predicted using a modified Hinckley-Von Mises yield criterion for orthotropic materials.

2. The initiation sites are symmetric and early crack trajectory from the hole confirms the dominant effect of shear induced plastic deformation at these locations. In the case of tension-tension fatigue, the crack trajectory finally becomes one that is perpendicular to the loading direction driven by normal stress. In the case of monotonic compression and compression-compression fatigue, the early crack trajectory is due to the effect of shear induced plastic deformation followed by fiber-matrix splitting along the loading direction.

3. The failure mode under monotonic tension is due to fiber fracture at the diametrical end points of the hole, perpendicular from the loading direction. Although past research has shown that plastic between 65-72 degrees from the vertical axis is possible, its effect is overshadowed by initial fiber fractures that lead to failure of the specimen into two halves. Thus, this monotonic tension failure mode is the only deviation from the failure mode of symmetric crack orientation as observed in the cases of monotonic compression, tension-tension fatigue and compression-compression fatigue.

ACKNOWLEDGEMENT

This research was conducted under an AFOSR grant. Dr. Walter Jones of AFSOR was the program monitor. His encouragement during the course of this research is gratefully acknowledged.

REFERENCES

- [1] Waddoups, M. E. , Eisenmann, J. R. , and Kaminski, B. E. , "Macroscopic Fracture Mechanics of Advanced Composite Materials," *J. compos. Mater.* **5**, 466-474 (1971).
- [2] Nuismer, R. J. , and Whitney, J. M. , "Uniaxial Failure of Composite Laminates Containing Stress Concentrations," *Fracture mechanics of composites*, ASTM STP **593**, 117-142 (1975).
- [3] Tsangarakis, N. , "Fatigue Failure of an Orthotropic Plate with a Circular Hole," *J.compos. Mater.* **18**, 47-57(1984).
- [4] Whitney, J. M. , and Nuismer, R. J. , "Stress Fracture Criteria for Laminated Composites Containing Stress Concentrations," *J. compos. Mater.* , 1008-1016 (1987).
- [5] Tsangarkis, N. , "The Notch-Fatigue Behaviour of Aluminium Composite Reinforced Unidirectionally with Silicon Carbide Fiber," *J. compos. Mater.* **8**, 253- 265 (1987).
- [6] Harmon, D. M. , and Saff, C. R. , "Damage Initiation and Growth in Fiber-Feinforced Metal Matrix Composites," *Metal Matrix Composites: Testing Analysis and Failure Modes*, ASTM STP **1032**, 237-250 (1989).
- [7] Harmon, D. M. , Saff, C. R. , and Graves, D. L. , "Strength Predictions for Metal Matrix Composites," *Metal Matrix Composites: Testing analysis and Faliure Modes*, ASTM STP **1032**, 222-236 (1989).
- [8] Newaz, G. M. , and Majumdar, B. S. , "Crack Initiation Around Holes in a Unidirectional MMC Under Fatigue Loading," *Engineering Fracture Mechanics*, vol. **42**, #4, pp 699-711, (1992).
- [9] Newaz, G. M. and Majumdar, B. S. , "Inelastic Deformation Mechanisms in SCS-6/Ti 15-3 MMC Lamina under Compression," NASA Contract Report # 191170, Cleveland, 1993.
- [10] Greszczuk, L. B. , "Stress Concentration and Failure Criteria for Orthotropic and Anisotropic Plate with Circular Openings," *Composite Materials: Testing and Design (Second Conference)*, ASTM STP **497**, 363-381 (1972).
- [11] EL-Soudani , S. M. , and Gambone, M. L. , "Strain Controlled Fatigue Testing of SCS- 6/Ti-6Al-4V Metal Matrix Composite," *in Proceedings of ASM symposium on metal matrix composites* (Edited by M. Gungor), Cincinnati, OH (1989).
- [12] Gayda, J. , Gabb, T. P. , and Freed, A. D. , "The Isothermal Fatigue Behavior of Unidirectional SiC/Ti Composite and the Ti-Alloy Matrix," NASA TM-101984, Cleveland, OH (1989).
- [13] Majumdar, B. S. , and Newaz, G. M. , "Inelastic Deformation of Metal Matrix Composites:Plasticity and Damage," *Phil. Mag.* ,pp 187-212, (1992).
- [14] Newaz, G. M. , and Majumdar, B. S. , "Deformation and Failure Mechanisms in MMCs," , ASME, AMD, Vol 122, pp 55-66 (1991).
- [15] Majumdar, B. S. , and Newaz, G. M. , "Inelastic Deformation of Metal Matrix Composites," *Proceedings of the 1991 HITEMP Conference*, NASA Lewis Research Center (1991).

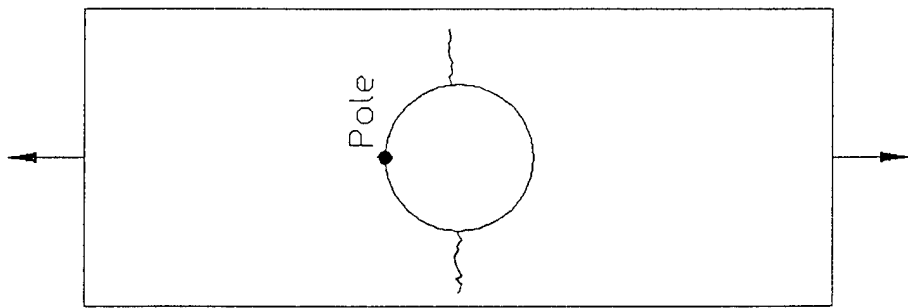


Fig. 1 Crack initiation and growth in unidirectional titanium MMC subjected to monotonic tension.

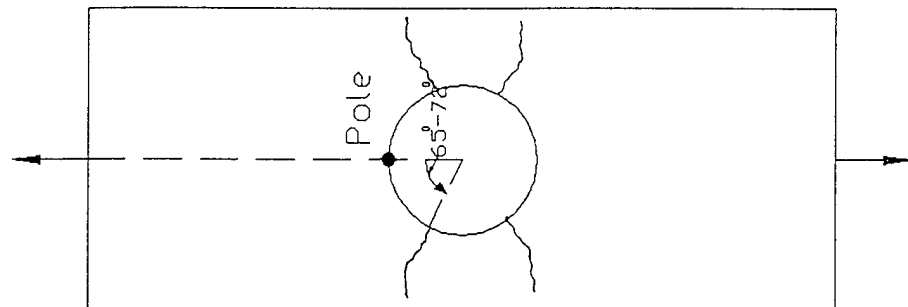


Fig. 2 Crack initiation and growth in unidirectional titanium MMC subjected to tension-tension fatigue.

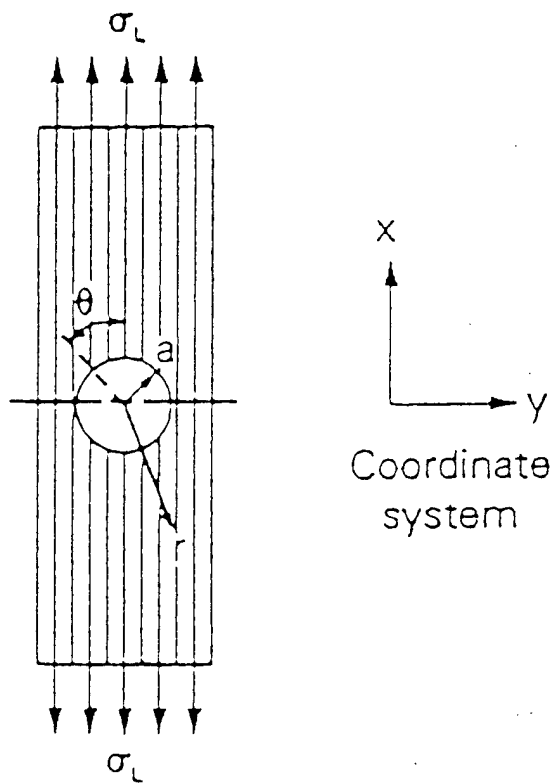


Fig. 3 Orthotropic composite plate containing a center hole (loading can be either in tension or in compression).

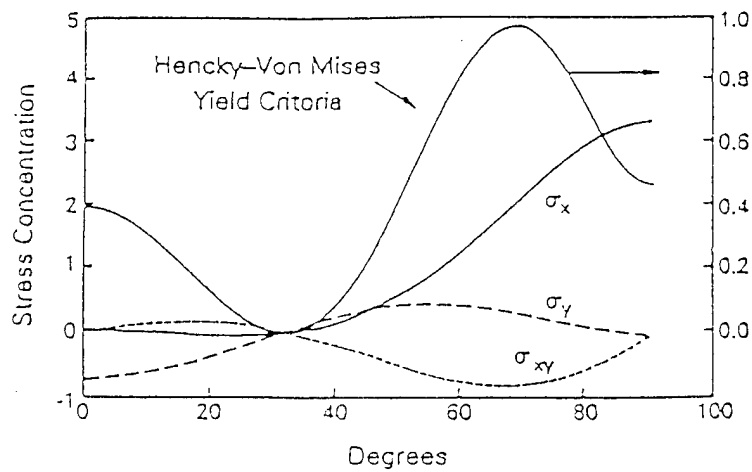


Fig. 4 Plot showing stress concentration and failure function [eq. (8)] as a function of angle.

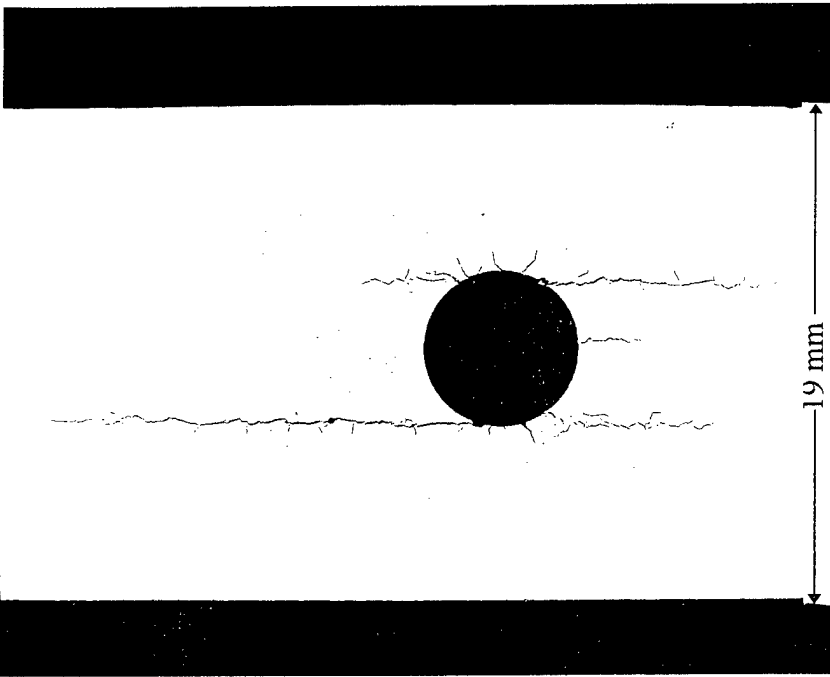


Fig. 5 Initiation of Four major symmetric cracks in unidirectional SCS-6/Ti 15-3 MMC under monotonic compression.

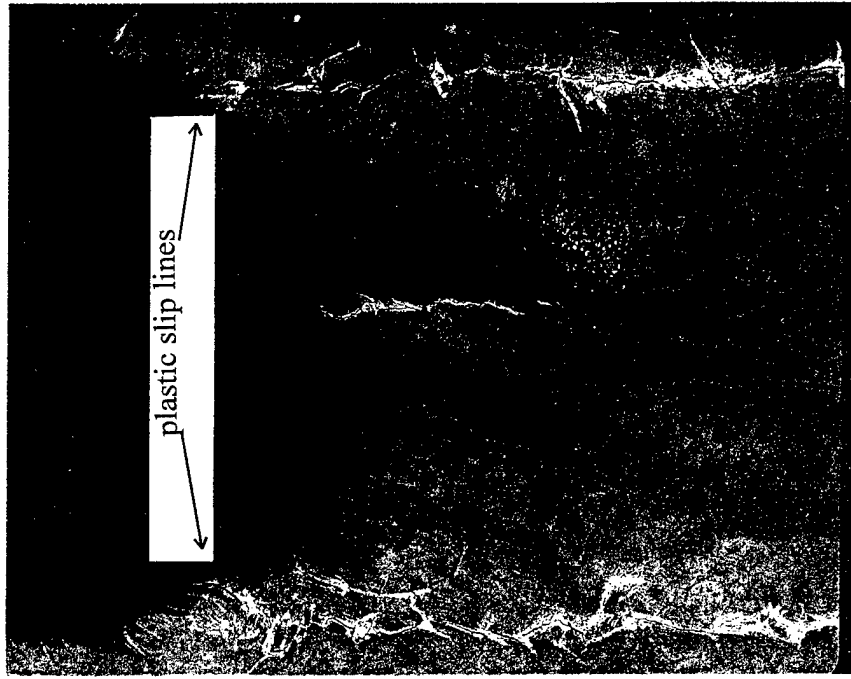
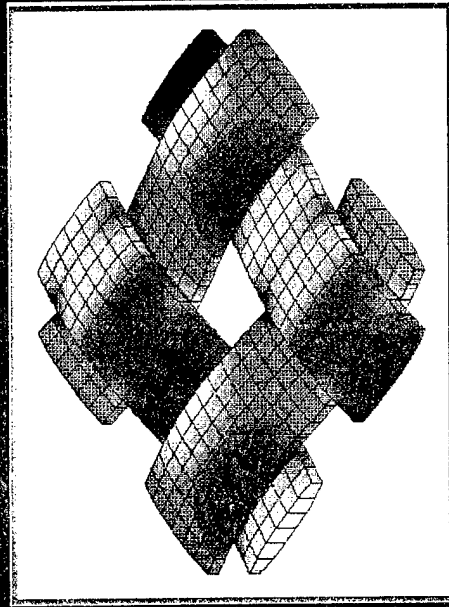


Fig. 6 Evidence of plastic deformation (slip lines) in SCS-6/Ti 15-3 unidirectional MMC under monotonic compression (25x magnification).

COMPOSITES '95:

Recent Advances
in Japan and the United States

EDITORS:
ISAO KIMPARA
HIROO MIYAIRI
NOBUO TAKEDA



Proceedings of the Seventh Japan-U.S.
Conference on Composite Materials

JAPAN SOCIETY FOR COMPOSITE MATERIALS

Editors:

I. Kimpara
H. Miyairi
N. Takeda

COMPOSITES '95:
Recent Advances
in Japan and
the United States

JAPAN-U.S.
CCM-VII
1995 KYOTO
JSCM

COMPOSITES '95:

Recent Advances
in Japan and
the United States

EDITORS:

ISAO KIMPARA

HIROO MIYAIRI

NOBUO TAKEDA

Proceedings of the Seventh Japan - U.S.
Conference on Composite Materials
June 19-22, 1995, Kyoto, Japan

Sponsored by
Japan Society for Composite Materials

Supported by
The Asahi Glass Foundation
Nippon Sheet Glass Foundation
for Materials Science
Research Foundation for Materials Science
Doshisha University

INELASTIC MECHANISMS AND RESPONSE OF UNIDIRECTIONAL MMC UNDER REVERSED FATIGUE LOADING

G. M. Newaz, Y.F. Wen and S.Q. Nusier
Wayne State University
Detroit, Michigan

and
N. Bonora
University of Cassino
Cassino, Italy

Abstract

In this investigation, load-controlled fully reversed fatigue ($R=-1$) of SCS-6/Ti 15-3 MMC unidirectional composite was investigated to determine its characteristic response and the associated inelastic mechanisms. In addition, the fatigue mechanisms were studied to determine the nature of damage evolution and to compare them to what is observed for zero-tension and tension-tension fatigue cycles. For elevated temperature response, it was found that multiple matrix cracking was a dominant damage mechanism under fully reversed fatigue loading and that the tension part of the cycle was a critical component in influencing life. The density of matrix cracks was higher than that is observed for the tension-tension cycling case for the same range of stress amplitude. Compression part of the cycle in a fully reversed loading may induce numerous cracks at the fiber-matrix interface which may then influence the development of many matrix cracks under fatigue loading. However, the fatigue performance under fully reversed condition ($R=-1$) was significantly higher than the zero-tension ($R=0$) case due to more effective crack opening in the latter case. The Hancock-Mackenzie effective plastic strain parameter is shown to have promise for correlating fatigue lives of unidirectional MMCs tested under two different R -ratios.

INTRODUCTION

Most components for structural applications of titanium-based high temperature metal matrix composites will be subjected to fatigue loading. Although fatigue response of MMC has been studied well and is a subject of continuing investigation [1-6], most investigations are confined to tension-tension fatigue loading. For this type of loading, side-tapered flat MMC specimens have been successfully used to evaluate the fatigue response and to determine the related inelastic mechanisms in the composites [6]. In this loading mode, depending on the stress level, various inelastic mechanisms have been observed. At high applied stress, interfacial debonding and reaction zone cracks seem to dominate as primary damage mechanisms. These microstructural deformation mechanisms and inelastic events eventually lead to fiber cracks and leads to specimen failure [5,6]. At intermediate stress levels, matrix cracking dominates as a dominant damage process, although interfacial debonding and reaction zone cracks are also present. The dominant damage mechanisms can be summarized in a generic fatigue-life plot as shown in Figure 1. These damage characteristics are similar at room temperature as well as under isothermal loading conditions.

In contrast to the efforts for the tension-tension characterization of MMCs under fatigue loading, understanding fatigue response under reversed loading has been minimal. In recent efforts, Lerch [5] studied the reversed fatigue response of MMCs using hour glass specimens. However, this specimen requires a large volume of material because of the cylindrical shape and they can be costly to machine. Therefore, utilization of the flat specimens need to be made to circumvent this expensive approach, although this may limit the applicability and evaluation of data for a certain range of stresses that are not too high to initiate premature buckling of the specimen. It is apparent then that there are two challenges related to evaluation of reversed fatigue response, namely, 1) conducting this type of tests with thin lamina poses difficulties due to the presence of the compression part of the cycle and 2) defining a stress regime in which reliable data can be gathered for the chosen specimen geometry. Premature buckling of the specimen can occur due to compression unless a proper stress regime is defined for the specimen geometry. These areas require considerable attention and research for MMCs. These challenges have been addressed recently [7]. Another important consideration is what influences the fatigue life of the MMCs.

In this investigation, response under fully reversed fatigue ($R=-1$) loading is evaluated for unidirectional MMCs to determine the associated damage mechanisms and the characteristic fatigue response. In addition, the fully-reversed response is compared with the zero-tension ($R=0$) response to determine the differences in their inherent characteristics. Also, attempts were made to correlate fatigue lives with a physically-based parameter e.g. Hancock-Mackenzie local effective plastic strain amplitude for the $R=0$ and $R=-1$ data.

EXPERIMENTAL ASPECTS

The material tested was an 8-ply unidirectional SCS-6/Ti 15-3 composite, approximately 2 mm thick, with a fiber volume fraction of 0.35. The SCS-6 fiber is a silicon carbide fiber having a diameter of about 140 microns. The Ti 15-3 matrix material is a metastable body-centered cubic (bcc) beta titanium alloy, the bcc phase being stabilized by vanadium. Unidirectional specimens were machined from a panel using electric-discharge machining (EDM) technique. All reversed fatigue testing was accomplished using 104 mmX10.2mmX2 mm rectangular specimens. The specimen gage section was 25.4 mm. Specimens used for the tension mode of testing are reduced cross-section specimens and are described in detail in the NASA report [2]. The $R=0$ data were obtained from the literature [8,9].

Specimens were gripped using friction grips and loaded in a servohydraulic testing machine for a frequency of 1 Hz. The R -ratio was -1 for fully reversed load-controlled fatigue loading. Tests were run both at room temperature (23C) as well as at elevated temperature (427C). The buckling guides were deliberately not used although the specimens experienced compression, primarily to determine the range of stresses within which reliable reversed fatigue data can be collected. Monotonic data for the specimens were taken from previous results obtained by the author and co-worker [2,7]. Several specimens were metallurgically polished to determine the nature of damage evolution. Optical microscopy was utilized to document the nature of reversed fatigue damage in the MMC specimens.

RESULTS AND DISCUSSION

The cyclic response of the composite is presented schematically for two different conditions at elevated temperatures (427C) for $R=0$ and $R=-1$ (Figures 2a and 2b). An important difference between the response for the $R=0$ and $R=-1$ cases is the fact that in the former case the composite hysteresis loops are parallel to each other reflecting no loss of stiffness for the most part of life. In the case of $R=-1$ loading, there is a tension and a compression component in the loading cycle. The tension part of the cycle shows stiffness loss, however, the compression part do not show any such change. Moreover, the compression part does not exhibit any hysteresis. These responses can be best understood in the context of the damage mechanisms observed in this composite for the different fatigue loading modes. This will be discussed later.

The data for the $R=0$ and $R=-1$ are plotted in the same life curve as shown in Figure 3. For the fully reversed case, it is clear that significantly improved lives were obtained compared with the zero-tension mode of testing. In most cases, for the same applied stress amplitude, up to one order of magnitude in improvement of life was obtained. The $R=0$ data presented in this paper are obtained from the literature. In our research, an investigation was undertaken to determine what was the controlling parameter for life performance, namely, is there a physically-based parameter that provides a real basis for life prediction?

The metallurgically polished specimens were examined using optical microscopy to determine the nature of inelastic mechanisms. For the $R=0$ case, we did not have direct confirmation of the damage mechanisms. But our experience with similar materials with 41 volume percent fibers showed that the typical damage was due to fiber-matrix interfacial separation or debonding (Figure 4) in the high to medium range of stresses $R=0.1$. In Regime II of fatigue (Figure 1), it was found that for these tests, there were matrix cracks as well [2]. Similar conditions are likely to be present for the $R=0$ case with 35 volume percent of fibers.

The fully reversed test showed a very interesting cracking morphology. Figure 5 illustrates the extensive amount of matrix cracks for a specimen cycled at a stress range of 1500 MPa (maximum stress of 750 MPa) at $R=-1$ at 427C. The crack density is much higher than observed for $R=0.1$ case at elevated or room temperature. It will be reasonable to assume that a similar condition occurs for the zero-tension case as well. The compressive part of the cycle in fully reversed fatigue may have been instrumental in nucleating additional cracks (compared with tension-tension case). Past investigation has shown [7] that extensive reaction zone cracks as well as fiber-matrix debonding occurred in compression. The elongated precipitates as shown in Figure 5 are believed to be alpha-particles that precipitated in-situ during the tests at 427C. The favored sites for the nucleation of these precipitates are imperfections, such as grain boundaries and dislocations.

In unnotched specimens in metals, plastic strain has been a key parameter for relating life performance to applied loading. Local plastic strain amplitude in fatigue has been an important variable affecting life. In unidirectional composites, the matrix between fibers are constrained such that even for load-controlled or stress-controlled case, the matrix or the fiber-matrix interface may be in a strain-controlled situation. Constrained multiaxial stress fields can build up

in MMCs with stiff fibers [10]. Hancock and Mackenzie [11] provided a law to investigate failures as a result of void nucleation. We conducted unit cell finite element computations (Figure 6) using the ABAQUS code to determine the level of plastic strains locally for the R=0 and the R=-1 cases using the effective plastic strain at failure for multiaxial stress states [11]:

$$\bar{\epsilon}_p = 1.65\epsilon_0 \exp\left[-\frac{1}{2} \frac{\sigma_{kk}}{\sigma}\right] \quad (1)$$

where ϵ_0 is plastic component of uniaxial failure of the matrix, σ_{kk} is the sum of the principal stresses and σ is the effective stress. The result is based on the Rice-Tracey void growth mechanism [12].

The total effective plastic strain amplitude is given by:

$$\Delta\bar{\epsilon}_p = 1.65\epsilon_0 \left[\exp\left(-\frac{1}{2} \frac{\sigma_{kk}^{\max}}{\sigma^{\max}}\right) - \exp\left(-\frac{1}{2} \frac{\sigma_{kk}^{\min}}{\sigma^{\min}}\right) \right] \quad (2)$$

where the max. and min. superscripts represent the maximum and minimum components of stresses for the fatigue cycle.

The life data were then replotted using the local axial effective plastic strain amplitude at the fiber-matrix interface at 427C. The results are presented in Figure 7. The R=0 and R=-1 data follows a trend and appears to indicate that local effective plastic strain amplitude may govern life in unnotched MMCs at elevated temperature. It may be noted that the strain expressed by Equation 1 represents effective plastic strain in the matrix at which local failure is expected (e.g. void formation and growth).

CONCLUSIONS

Based on this investigation, the following conclusions may be reached:

1. Fully reversed loading under load controlled-condition can be less severe in terms of life performance compared with zero-tension and tension-tension cycling for unidirectional MMCs.
2. The hysteresis response is significantly different for R=0 and R=-1 loading profiles due to the specific mechanisms that develop during fatigue loading and local energy dissipation characteristics.
3. For R=-1 case, the compressive part of the loading cycle is likely to produce nucleation sites in the coating or reaction zone of the fiber. The tension part of the cycle influences the opening of the matrix cracks and in producing a higher matrix crack density from these nucleation sites.

4. In Regime II, for R=0, the damage mechanism is primarily due to fiber-matrix debonding and limited matrix cracking. Consequently, stiffness loss for axial loading is not pronounced as in the R=-1 case.

5. Local effective plastic strain amplitude as calculated using the Hancock and Mackenzie expression appears to correlate life data for different R-ratio fatigue data.

ACKNOWLEDGEMENT

The author would like to acknowledge the financial support of AFOSR for this research program. Encouragement of Dr. Walter Jones is gratefully acknowledged.

REFERENCES

1. Gabb, T.P., Gayda, J. Lerch, B.A. and Halford, G.R., "The Effect of Matrix Mechanical Properties on Unidirectional SiC/Ti Composite Fatigue Resistance", Scripta Metallurgica, Vol. 25, 1991, pp. 2879-2884.
2. Majumdar, B.S. and Newaz, G.M., " Isothermal Fatigue Mechanisms in Ti-Based Metal Matrix Composites ", NASA Contractor Report No. 191181, Lewis research center, Cleveland, 1993
3. Gabb, T.P., Gayda, J., and Mackay, R., "Isothermal and Non-Isothermal Fatigue Behavior of a Metal Matrix Composite" J. of Composite Materials, Vol. 24, 1990, pp. 667-686.
4. Bartolotta, P.A. and Brindley, P.K., High temperature fatigue behavior of a SiC/Ti-24Al-11Nb Composite, NASA Tech. Memorandum No. 103157, 1990
5. Lerch, B.A., Verrilli, M.J. and Halford, G.R., " Fully-Reversed Fatigue of a MMC ", Proc. of American Society of Composites, Eighth Technical Conference, G.M. Newaz, Editor, Technomic Publishing Co., Lancaster, PA, 1993, pp. 388-396.
6. Majumdar, B.S. and Newaz, G. M., " Mechanisms of Fatigue Damage and Failure of a SiC-6/Ti 15-3 Composite", Mechanisms and Mechanics of Composite Fracture, Proceedings of ASM 1993 Materials Congress, Eds., R.B. Bhagat, S.G. Fishman, and R.J. Arsenault, 1993, pp. 77-90.
7. Newaz, G. M. and Majumdar, B.S., " Inelastic deformation Mechanisms in SiC6/Ti 15-3 MMC Lamina Under Compression", NASA Contractor Report No. 191170, NASA-LeRC, Cleveland, 1993
8. Gayda., and Gabb, T.P. "Isothermal Fatigue Behavior of a Transverse SiC/Ti-15-3 Composite at 426C, NASA Tech. Memorandum No. 103686, 1991.
9. Lerch, B.A., " Fatigue behavior of SiC/Ti 15-3 Laminates, NASA Conference Publication No. 10051, HITEMP Review, 1990, pp. 35.1-35.8.

10. Gunawardena, S.R., Jansson, S. and Leckie, F.A., "Transverse Ductility of MMC", in Failure Mechanisms in High Temperature Composite Materials, Eds. G.K. Haritos, G. Newaz, and S. Mall, Proc. of ASME Winter Annual Meeting, AD-Vol. 22/AMD-Vol. 122, 1990, pp. 23-30.

11. Hancock, J.W. and Mackenzie, A. C., " On the Mechanisms of Ductile Fracture in High Strength Steels Subjected to Multiaxial States of Stress", J. of Mechanics and Physics of Solids, Vol. 24, 1976, pp. 141-169.

12. Rice, J.R. and Tracey, D.M., " On the Ductile Enlargement of Voids in Triaxial Stress Fields", J. Mechanics of Physics and Fields", J. Mechanics and Physics of Solids, Vol. 17, 1969, pp.201-217.

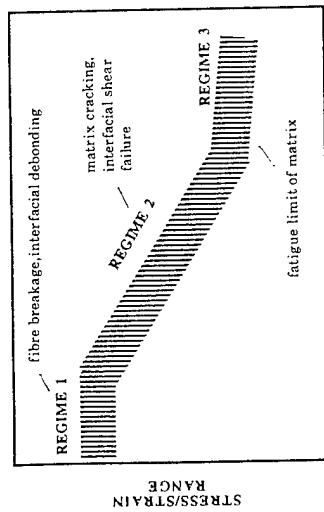


Figure 1. Fatigue regimes for composite materials.

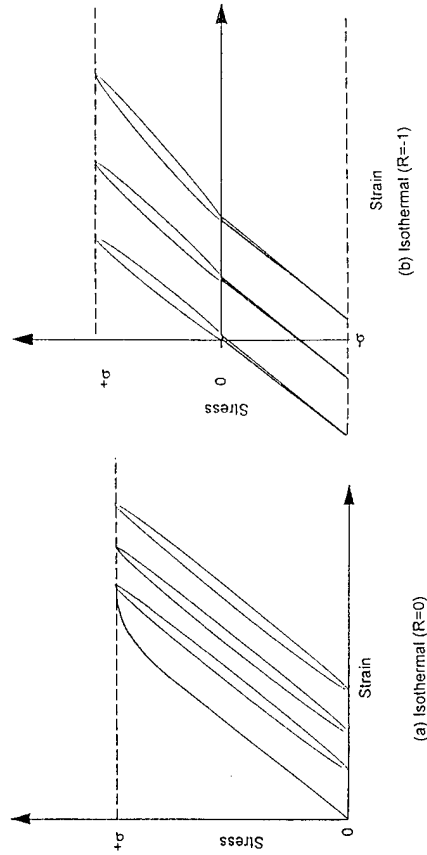


Figure 2. Typical hysteresis response for a) R=0 and b) R=-1 in unidirectional MMC.

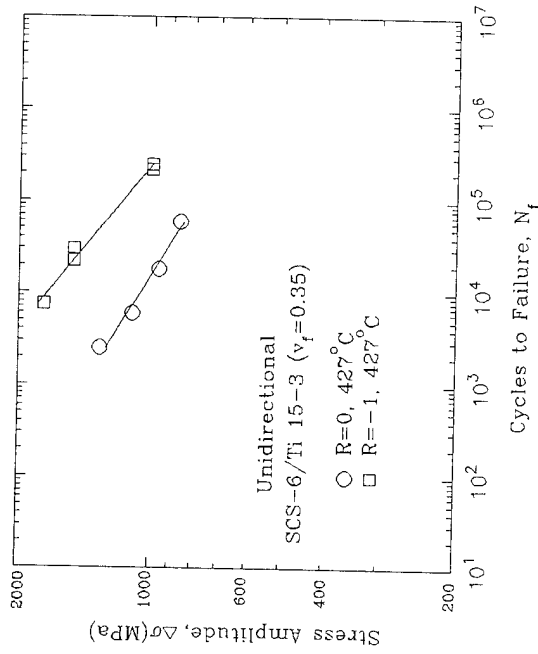


Figure 3. Fatigue lifetime plot for unidirectional MMC.

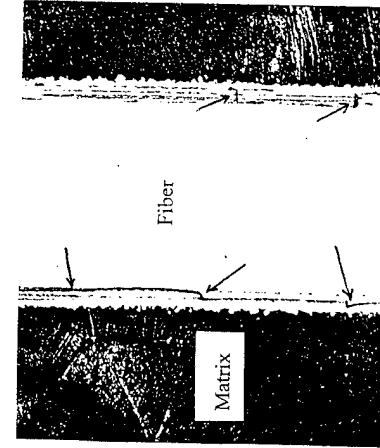


Figure 4. Interfacial cracking in R=0.1 isothermal (427°C) fatigue specimen for 1000 MPa stress range (magnification 500X).

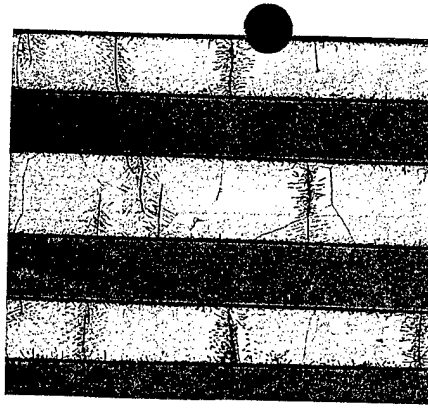


Figure 5. Matrix cracks (with alpha-precipitates) in R=-1 isothermal (427°C) fatigue specimen at 1500 MPa stress range (magnification 100X).

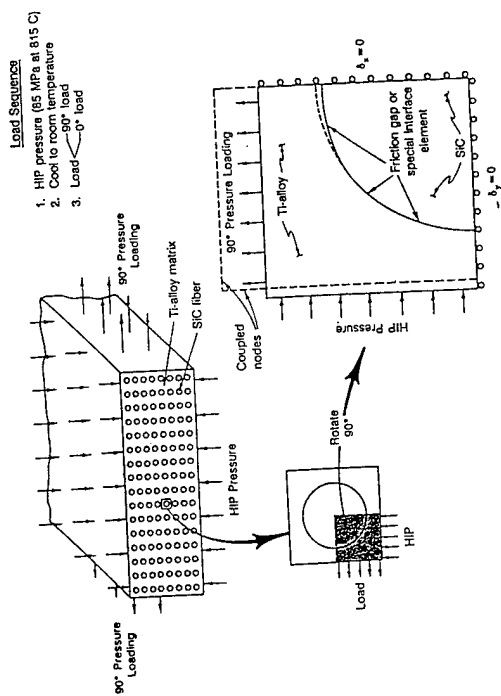


Figure 6. Computational unit cell finite element model for unidirectional MMC.

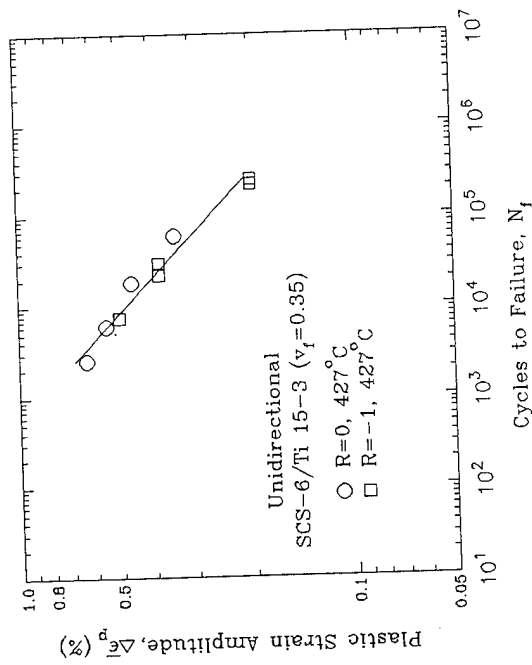


Figure 7. Correlation of fatigue data with two different R-ratios using the Hancock-Mackenzie effective plastic strain.